



Contents lists available at ScienceDirect

Precambrian Research

journal homepage: www.elsevier.com/locate/precamres

Late Ediacaran geological evolution (575–555 Ma) of the Djanet Terrane, Eastern Hoggar, Algeria, evidence for a Murzukian intracontinental episode

Nassima Fezaa^a, Jean-Paul Liégeois^{b,*}, Nachida Abdallah^c, El Hadi Cherfouh^d, Bert De Waele^e, Olivier Bruguier^f, Aziouz Ouabadi^c

^a ISMAL/Université d'Alger, Bois des Cars, Dély Ibrahim, Alger, Laboratoire de Géodynamique, Géologie de l'ingénieur et Planétologie, USTHB, Algeria

^b Isotope Geology, Royal Museum for Central Africa, B-3080 Tervuren, Belgium

^c USTHB, Laboratoire de Géodynamique, Géologie de l'ingénieur et Planétologie, Faculté des Sciences de la Terre, Aménagement du Territoire et de la Géographie, BP 32, El Alia, Bab Ezzouar, 16111 Alger, Algeria

^d Faculté des Sciences Biologiques et des Sciences Agronomiques, Université Mouloud Mammeri de Tizi-Ouzou, Laboratoire de Géodynamique, Géologie de l'ingénieur et Planétologie, USTHB, Algeria

^e SRK Consulting, 10 Richardson Street, West Perth, WA 6005, Australia

^f Géosciences Montpellier, Université de Montpellier II, F-34095 Montpellier, France

ARTICLE INFO

Article history:

Received 18 September 2009

Received in revised form 25 February 2010

Accepted 5 May 2010

Keywords:

Hoggar

Murzuq craton

Murzukian intracontinental event

U–Pb zircon

Sr–Nd isotopes

Metacraton

ABSTRACT

The Eastern Hoggar is by far the least well known part of the Tuareg Shield. It is composed, from west to east, of the Aouzegueur, Edembo and Djanet Terranes. The Djanet Terrane is the easternmost Hoggar terrane and comprises a greenschist-facies clastic sedimentary sequence, the Djanet Group, intruded by granitoids. Laser ablation (LA-) ICP-MS U–Pb zircon ages of detrital zircons from these sediments yield a large range of ages similar to ages known in Central and Western Hoggar; the youngest is 590 ± 10 Ma (2σ), which is the maximum age of deposition of the Djanet Group. The Djanet Group is intruded by the Djanet Batholith (571 ± 16 Ma), by high-level subcircular plutons such as the Tin Bedjane Pluton (568 ± 5 Ma) and finally by the felsic Tin Amali Dyke Swarm (558 ± 5 Ma), all ages being SHRIMP U–Pb zircon. The deposition and metamorphism of the Djanet Group thus occurred between 590 Ma (the age of the youngest detrital zircons analyzed in the Djanet Group) and c. 570 Ma (the age of intrusive granitoids). Nd T_{DM} two-stage model ages (1.30–2.03 Ga), initial $^{87}\text{Sr}/^{86}\text{Sr}$ ratios (0.7035–0.7095) and ε_{Nd} (–3 to –11) of the three intrusive suites, all being high-K calc-alkaline in composition, indicate mainly an old, Rb-depleted continental source. Migmatization in the adjacent Edembo Terrane is dated at 568 ± 4 Ma (U–Pb zircon SHRIMP age), contemporaneous with the intrusion of the Djanet plutons. Rocks and events in the Edembo and Djanet Terranes are all intracontinental. We propose that the Djanet Terrane lies on the boundary of a craton located to the north-east, that we defined here as the Murzuq craton. The existence of the Murzuq craton is supported by sedimentary and geophysical data. We suggest that the deformation of Eastern Hoggar occurred 575–555 Ma, due to the indentation of the Murzuq craton and has no link with the older convergence with the West African craton as was the case for the central and western parts of the Tuareg Shield. This determines a late Ediacaran intracontinental Murzukian event that probably also occurred to the east in the Tibesti area.

© 2010 Elsevier B.V. All rights reserved.

1. Introduction

The Tuareg Shield (500,000 km²) is a Cenozoic dome composed of Precambrian lithologies unconformably overlain by subhorizontal Palaeozoic sediments (Fig. 1A). Most of it lies in Algeria (Hoggar)

and extends SW into Mali (Adrar des Iforas) and SE into Niger (Air mountains). The Tuareg Shield comprises abundant Archaean and Palaeoproterozoic terranes (e.g. Peucat et al., 1996, 2003; Bendaoud et al., 2008) sometimes well-preserved (In Ouzzal terrane; Ouzegane et al., 2003) and sometimes reactivated during the Pan-African orogeny (630–580 Ma; LATEA metacraton, Liégeois et al., 2003; Bendaoud et al., 2008). Neoproterozoic juvenile oceanic or continental terranes are also common, generally predating the main c. 600 Ma collision period, with ages ranging from 870 to 650 Ma (Caby et al., 1982; Caby and Andreopoulos-Renaud, 1987; Liégeois et al., 1987, 1994; Henry et al., 2009).

The Tuareg Shield has been subdivided into 23 terranes (Black et al., 1994) superimposed on the former three-folds structure

* Corresponding author. Tel.: +32 2 650 2252/42; fax: +32 2 650 2252.

E-mail addresses: fezaanassima@yahoo.fr (N. Fezaa), jean-paul.liegeois@africamuseum.be, jplieg@ulb.ac.be (J.-P. Liégeois), a.nachida@yahoo.fr (N. Abdallah), echerfouh@yahoo.fr (E.H. Cherfouh), bdewaele@srk.com.au (B. De Waele), bruguier@gm.univ-montp2.fr (O. Bruguier), ouabadi@yahoo.fr (A. Ouabadi).

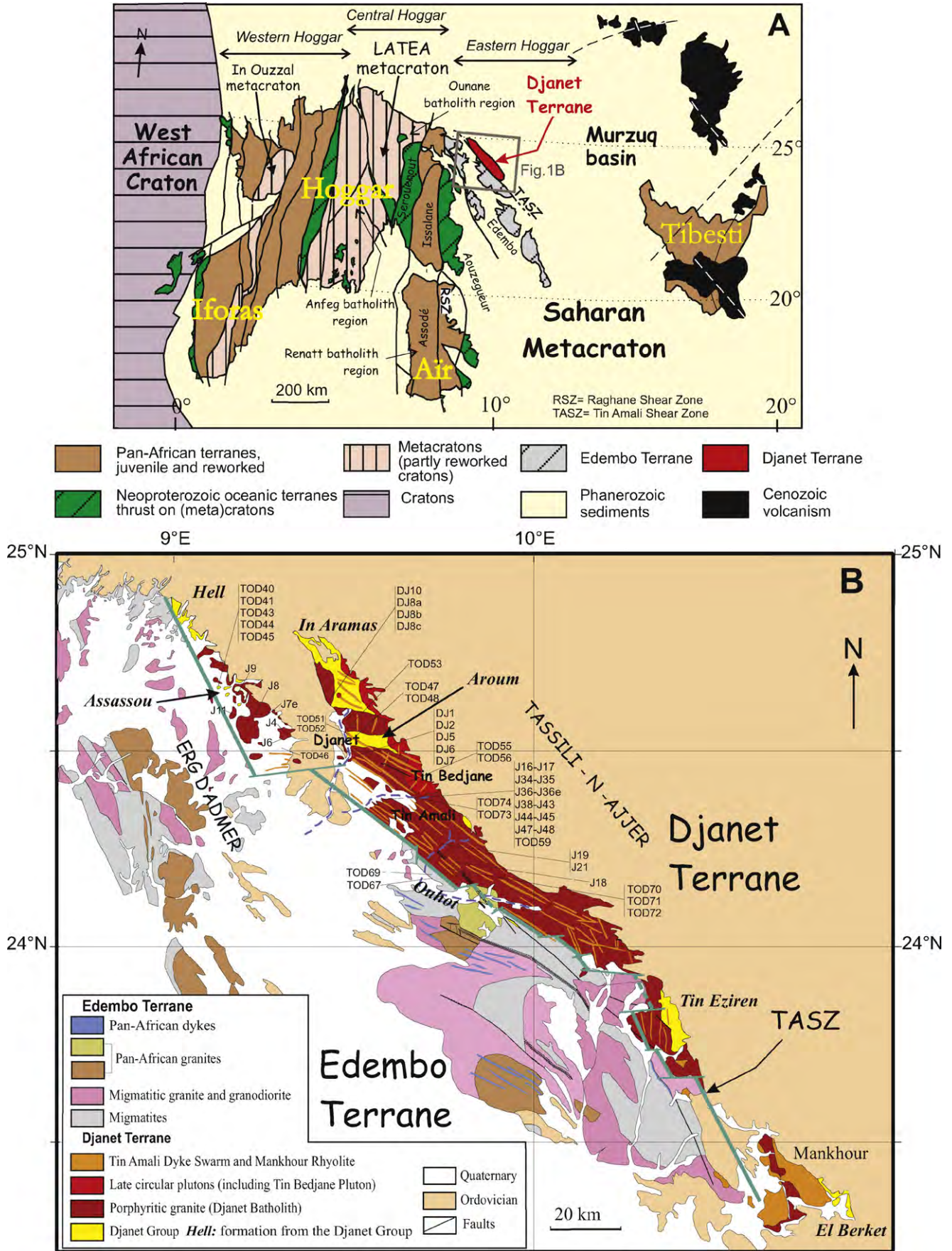


Fig. 1. (A) The different terranes of the Tuareg Shield (modified from Black et al., 1994); (B) Geological map of the Djanet Terrane and the eastern part of the Edembo Terrane (modified from Le Caignec et al., 1957 and observations from the authors).

of Western, Central and Eastern Hoggar (Fig. 1A; Bertrand and Caby, 1978). This former structure however remained useful, the Western Hoggar being mainly composed of terranes generated and shaped during the Neoproterozoic (with the exception of the In Ouzzal Terrane; Ouzegane et al., 2003), the Central Hoggar being a Eburnean domain dissected and invaded by granites during the Pan-African convergence (Liégeois et al., 2003) and the Eastern Hoggar, subject of this study, being different and “exotic” (Caby and Andreopoulos-Renaud, 1987), although poorly known. The Eastern Hoggar is bounded to the west by the major Raghane shear zone (Fig. 1A), which is also marking the western boundary of the Saharan metacraton (Liégeois et al., 1994; Abdelsalam et al., 2002).

To the west of the Raghane shear zone, the orogenic events that affected the Western and Central Hoggar are related to the collision with the c. 2 Ga Eburnean domain of the West African Craton (WAC) during the Pan-African orogeny (630–580 Ma; Black et al., 1979; Liégeois et al., 1987, 2003; Jahn et al., 2001; Caby, 2003). By contrast, the Eastern Hoggar, located about 1000 km east of the suture with the WAC, is considered to have escaped most of the effect of the Pan-African collision (Caby and Andreopoulos-Renaud, 1987; Black et al., 1994). The Eastern Hoggar was considered to be “cratonized” at 730 Ma, based on the U–Pb on zircon dating of undeformed granite within the Aouzegueur Terrane, the westernmost terrane in the Eastern Hoggar (Fig. 1A; Caby and Andreopoulos-Renaud, 1987). A recent study in the Aouzegueur Terrane (Henry et al., 2009) confirms the existence of pre-Pan-African Neoproterozoic granitoids (c. 790 Ma) but also the existence of granitoids at c. 590 Ma and c. 550 Ma, all being located not far from the Raghane shear zone. This indicates a more complex story for the Aouzegueur Terrane than previously thought.

Concerning the target of this study, the Djanet Terrane, the easternmost terrane of the Tuareg Shield, as well as the western neighbour Edembo Terrane (Fig. 1A), no recent data were available, the only existing documents being the reconnaissance geological maps done half a century ago by the BRMA and accompanying unpublished reports (e.g. Le Caignec et al., 1957 for the Djanet area). A major feature was the juxtaposition of these two terranes with contrasted metamorphisms (greenschist-facies in Djanet, amphibolite-facies in Edembo; Black et al., 1994). The crustal architecture and the overall geological evolution of this area are unknown although their knowledge is essential for understanding the formation of Africa during the Neoproterozoic, including that of the enigmatic Saharan metacraton and for throwing amares towards the geological evolution of NE Africa. There the eastern boundary of the Saharan metacraton was involved in the collision with the Arabian–Nubian Shield at the same period of time (Küster et al., 2008 and references therein).

In this study, we will give field information on the relation existing between the different lithologies, we will date the sedimentary, magmatic and metamorphic events using U–Pb on zircon punctual methods (SHRIMP and LA-ICP-MS), determine geochemically and isotopically the protoliths of the metasediments and the nature of the magmatism. We will show that all the events occurred in an entirely intracontinental environment within the mostly post-Pan-African 590–550 Ma age range. We will propose a model where the Murzuk basin, located just to the east of the Djanet Terrane, is underlain by a cratonic lithosphere depicted by geophysics. This Murzuk craton, whose existence is proposed here for the first time, would have been responsible for the observed late geological evolution of the Djanet Terrane and probably also in the Edembo Terrane as well as to the east in Chadian the Tibesti. We will name in consequence this late Ediacaran intracontinental event the Murzukian episode. Its existence is a big change with the former idea of a Cryogenian cratonization and its knowledge will most probably be a major step in the under-

standing of the final amalgamation of Gondwana in northern Africa.

2. Geological background

The Tuareg Shield comprises two metacratonic areas, i.e. Archaean to Palaeoproterozoic domains partly reactivated during the Pan-African orogeny the In Ouzzal and LATEA metacratons (Caby, 1996; Liégeois et al., 2003; Fig. 1A), in addition to the Saharan metacraton to the east. The latter is very poorly known in the Tuareg Shield and is the subject of the present study. The In Ouzzal metacraton is characterized by well-preserved c. 2 Ga ultra-high-temperature granulitic metamorphic rocks (up to 1050 °C for 11 kbar; Ouzegane et al., 2003). The Pan-African effects were limited there to movements along major shear zones bounding the terrane and to brittle faults inside the terrane, along which a few granitic plutons intruded (Ouzegane et al., 2003). The LATEA metacraton is an assembly of four terranes (LATEA stands for Laouni/Azrou n’Fad/Tefedest/Egéré-Aleksod, the names of the four terranes) that behaved coherently during the Pan-African orogeny, and that were little deformed (Liégeois et al., 2003). They are characterized by Archaean and Palaeoproterozoic amphibolite- to granulitic-facies metamorphic rocks accompanied by restricted late magmatism dated at c. 1.9 Ga in the NW (Peucat et al., 2003) and at c. 2.1 Ga in the SE (Bendaoud et al., 2008). The Pan-African effects are more pervasive than in the In Ouzzal metacraton but the original Palaeoproterozoic parageneses are often well-preserved. Neoproterozoic events correspond to collisions with Neoproterozoic oceanic terranes at several periods including c. 685 Ma (Liégeois et al., 2003) and preserved as thrust sheets and by the main Pan-African orogenic event typified by reactivation of shear zones and intrusion of granitoids accompanied by greenschist- to amphibolite-facies metamorphism during 630–580 Ma (Bertrand et al., 1986; Liégeois et al., 2003; Abdallah et al., 2007; Bendaoud et al., 2008). The Temaguessine circular, high-level pluton, dated at 582 ± 5 Ma marks the end of Pan-African deformation in the LATEA metacraton (Abdallah et al., 2007). However, later reactivations of shear zones accompanied by magmatism (Taourirt province) occurred at c. 525 Ma and are attributed to distant stress field (Azzouni-Sekkal et al., 2003).

East of LATEA (Central Hoggar), the Assodé-Issalane Terrane comprises high-temperature amphibolite-facies rock units, widespread potassic leucogranite and high-K calc-alkaline batholiths (Liégeois et al., 1994). The Assodé-Issalane Terrane probably corresponds to an extensively reactivated part of LATEA (Liégeois, 2005). The Assodé-Issalane Terrane is limited to the east by the Raghane shear zone (Fig. 1A), which is the western boundary of the Eastern Hoggar domain and of the Saharan metacraton (Liégeois et al., 1994; Abdelsalam et al., 2002; Henry et al., 2009).

East of the Raghane shear zone, the Eastern Hoggar (as defined by Bertrand and Caby, 1978), along which the Tiririne Belt extends (Bertrand et al., 1978), is composed of three contrasted NW–SE oriented terranes (Black et al., 1994; Fig. 1A). These terranes are: (1) the Aouzegueur Terrane, composed of Neoproterozoic oceanic rocks thrust eastward (Boullier et al., 1991; Liégeois et al., 1994) during the 800–650 Ma period with granitic plutons intruding these structures at c. 600 Ma (Henry et al., 2009); (2) the Edembo Terrane, composed of an amphibolite-facies metamorphic basement intruded by various granitoids and (3) the Djanet Terrane, composed of greenschist-facies sediments intruded by high-K calc-alkaline granites (Black et al., 1994). No oceanic-related rocks are known in the two latter terranes. The Aouzegueur terrane relates to a distinct story linked to the geological convergence that occurred to the west (Henry et al., 2009) and will not be described further here.

2.1. The Djanet Terrane

The Djanet Terrane is separated from the Edembo Terrane to the west by the NW–SE oriented Tin Amali Shear Zone (Figs. 1A, B and 2A). To the east, the Djanet Terrane is unconformably overlain by the late Cambrian to early Ordovician Tassilis sandstones (Fig. 1A and B; Ajjer Formation; Beuf et al., 1971). These Tassilis sandstones constitute the western margin of the Murzuq Basin (Fig. 1A), which extends into Libya on a surface of more than 350,000 km² without any Precambrian outcrops before reaching the Tibesti region (Fig. 1A).

The Djanet Terrane is composed of a greenschist-facies sedimentary sequence (the Djanet Group; Fig. 2A–C), intruded by an extensive porphyritic granite (the Djanet Batholith; Fig. 2D), by a series of high-level circular plutons, including the Tin Bedjane Pluton (Fig. 2E) and finally by the Tin Amali Dyke Swarm (Fig. 2F and G). The latter crosscuts all the granites and is oriented NW–SE parallel to the Tin Amali Shear Zone. A rhyolitic unit, the Mankhour Rhyolite, was probably fed by the Tin Amali Dyke Swarm (Fig. 1B).

The Djanet Group is mainly a clastic series (Fig. 2A–C) comprising slates, quartzites and conglomerates (Fig. 2B) interleaved with decimeter to meter thick sills of pyroxene-amphibole andesite and minor amounts of more acid compositions, up to rhyolite. These sills are often boudinaged within the sedimentary sequence. Its thickness is not known. The Djanet Group outcrops in six geographically distinct areas at In Aramas, Aroum, Assassou, Hell, Tin Eziren and El Barkat (Fig. 1B). They display mostly similar metasediments with some peculiarities in each location. No stratigraphical correlations can be setup with the present knowledge. The Aroum area is characterized by a thick conglomeratic bed that contains mainly intraformational pebbles but also a few granitic and aplitic pebbles (Le Caignec et al., 1957). The Hell area seems to have a slightly higher metamorphic grade, although still in the greenschist-facies (Le Caignec et al., 1957). At El Barkat, the Djanet Group is overlain or crosscut by the Mankhour Rhyolite. Contact metamorphism, marked by andalusite schists, developed around the Djanet Batholith and some small plutons. In the Djanet Group, open folds are the rule but nearly recumbent fold closures can be observed at the cm-scale. The orientation of the cleavage is variable, from N30°W to N80°E oriented. Dextral C/S structures are observed (Fig. 2C).

Petrographically, the Djanet metasediments are relatively homogeneous, differing essentially by the grain size. They are made of quartz, feldspar and mica (biotite and muscovite) from silts (grain size of <0.06 mm) to sandstones (grain size mostly <0.1 mm); conglomerates are made of a matrix similar to former rocks containing large crystals of quartz and feldspar and mm- to cm-size pebbles made up of aggregates of quartz, feldspar and mica, sometimes being monomineralic. Alternation of these different facies can be seen under the microscope and at the outcrop scale.

The Djanet Batholith (Fig. 2D) has intruded the Djanet Group and includes deformed and schistosed rocks from the Djanet Group. It develops contact metamorphism within the Djanet Group (e.g. andalusite) generally slightly deformed. Boudinaged dykes or sills of the Djanet granite have been observed within the Djanet Group indicating dextral strike-slip movements. The Djanet Batholith was in turn intruded by the circular plutons and the Tin Amali Dyke Swarm. It is dominated by coarse-grained porphyritic monzogranite that shows K-feldspar crystal accumulation structures and is rich in amphibole and biotite. Its normative composition spreads within the monzogranitic field (Fig. 3). K-feldspar is often perthitic and forms megacrysts up to 10 cm. Plagioclase is oligoclase (An₃₀₋₁₈), with granodioritic sample J8 containing andesine (An₃₄₋₃₁). Monzogranitic sample J6 contains, in addition to oligoclase, some albite (An₈₋₁). Amphibole is ferro-hornblende and a ferro-tschermakite-hornblende (electron microprobe determina-

tions). Accessory minerals are apatite, zircon, allanite and opaque oxides. Enclaves are abundant (Fig. 2G) and are of four types: (1) microgranular mafic magmatic amphibole biotite enclave (MME); sample DJ7 is a quartz monzodiorite (Fig. 3) with quartz ocelli rimmed mainly by amphibole, indicating magma mixing-mingling; (2) granular magmatic amphibole biotite enclaves ranging from intermediate to acid normative composition (Fig. 3): quartz-diorite (DJ8a), quartz monzodiorite (J7E, DJ8c), granodiorite (DJ2) and monzogranite (DJ5); (3) basic mica and plagioclase-rich enclaves sometimes strongly enriched in biotite (DJ8b and J8e) rarely with amphibole (TOD73); and (4) Djanet Group xenoliths, are represented by sample J11, made of quartz, mica and plagioclase. In magmatic enclaves and biotite-rich enclaves, allanite is common and other accessory minerals are zircon, oxides and apatite.

Circular plutons have sharp contacts with country-rocks. The Tin Bedjane Pluton, 12 km in diameter (Fig. 2E), and partly covered by the Tassilis sandstones (Fig. 1B), is a coarse-grained syenogranite (Fig. 3) with large rounded quartz crystals, perthitic K-feldspar, rare biotite and late amphibole. The small Djilouet pluton (1 km wide), near the town of Djanet, is composed of microgranite with feldspar and quartz phenocrysts with minor biotite and muscovite. It is associated with a pneumatolytic mineralization (cassiterite greisen and crosscutting cassiterite–wolframite quartz dykes; Le Caignec et al., 1957).

The Tin Amali Dyke Swarm is widespread and dense (Figs. 1B and 2F). The dykes are mostly NW–SE oriented but west of Djanet, they trend E–W, parallel to Djanet Group cleavage. SE of Djanet, two directions of dykes are observed, N–S dykes being crosscut by E–W dykes. The N–S dykes are discontinuous, being displaced by E–W brittle faults towards the east (dextral). These dykes crosscut all the granite plutons and are the last magmatic manifestation within the Djanet Terrane before Cenozoic volcanism. The dykes (Fig. 2F) have a dominant granodiorite to monzogranite composition although some analyses fall in the fields of monzodiorite and syenogranite (Figs. 2G and 3). The Fe–Mg minerals are biotite, amphibole and rarely pyroxene (e.g. TOD46). Accessory minerals include abundant oxides, zircon and apatite.

As a whole, the Djanet magmatism appears to have intruded during and at the end of the deformation of the Djanet Group, when ductile and under greenschist conditions for the Djanet Batholith and when brittle for the Tin Amali Dyke Swarm. Considering the relative volume of the Djanet batholith and of the Djanet Group, largely in favour of the former (Fig. 1B), it can be proposed that at least a part of the heat flow needed for the greenschist-facies metamorphism was brought by the Djanet Batholith.

2.2. The Edembo Terrane

The Edembo Terrane is NW–SE elongated and bounded by shear zones adjacent to the Djanet Terrane (Fig. 1A and B). It is characterized by amphibolite-facies metamorphism with abundant migmatites (Ouhot Complex; Fig. 2H) and strong ductile deformation. Lithologies include biotite micaschists, metagreywacke with pebbles, phlogopite marble, hornblende metabasalt, and migmatitic gneiss. Leucosomes can be dm-thick (Fig. 2H) evolving towards pockets of two-mica garnet-bearing granite with blue quartz. Garnet is abundant in many lithologies. High-temperature stretching mineral lineation is generally subhorizontal and N140°E oriented. Schistosed/migmatitic corridors of high-temperature ductile deformation have the same direction with a slope of 60–85°W. They indicate a dextral movement. Outside these corridors, the ductile deformation has more variable directions. The shear zone that separates the Edembo terrane from the Djanet Terrane is highly migmatitic. When properly seen, mostly to the south-east of Djanet, its foliation is N130°–140° oriented with a slope of about 70°E. The stretching mineral lineation

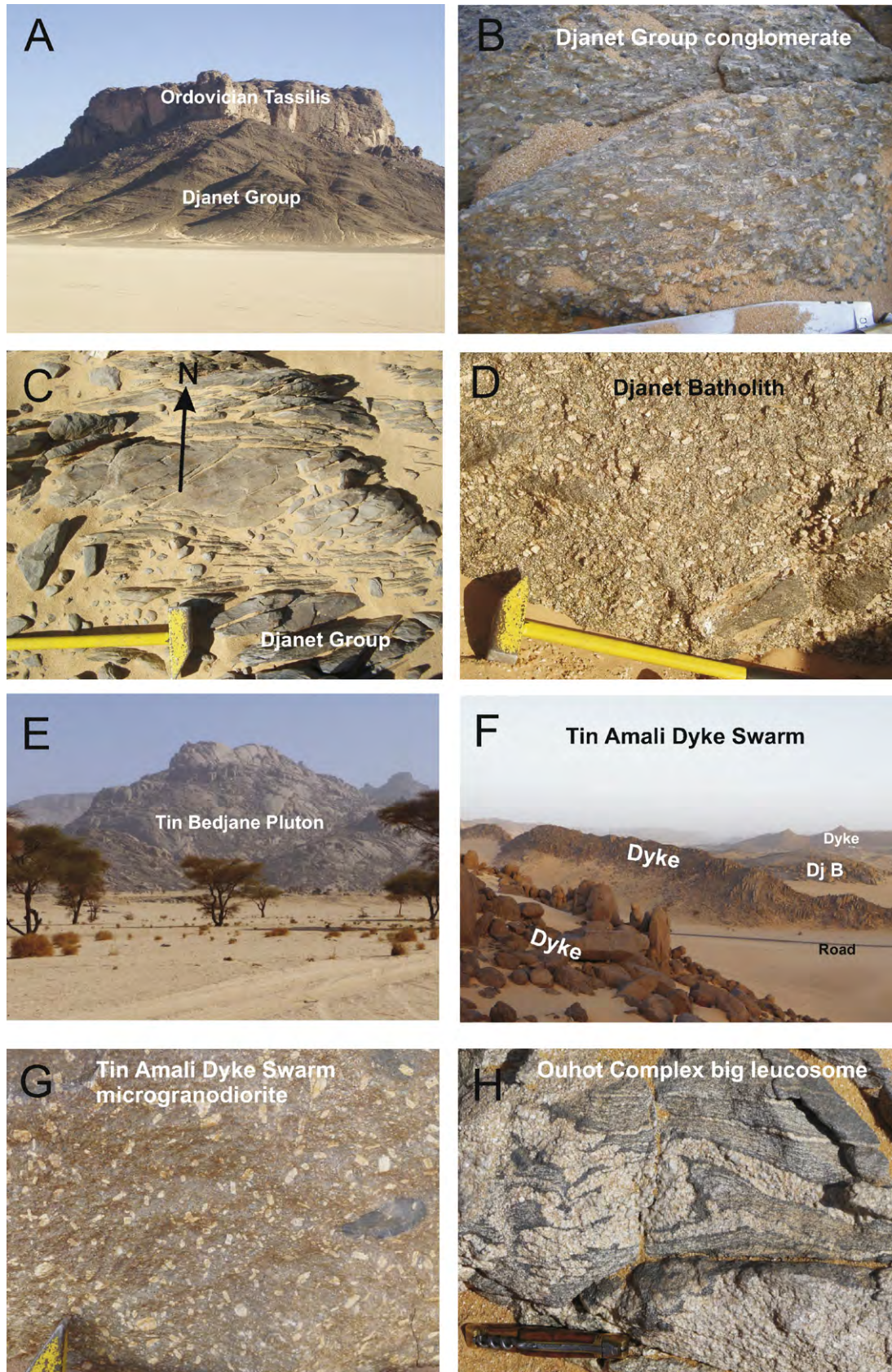


Fig. 2. Pictures of (A) the unconformity of the Ordovician sandstones (Tassilis) on the Djanet Group; (B) conglomerate from the Djanet Group; (C) Deformation in the Djanet Group; (D) porphyritic granite and mafic magmatic enclaves in the Djanet Batholith; (E) Tin Bedjane Pluton; (F) landscape view showing the volume of the Tin Amali Dyke Swarm; DjB = Djanet Batholith, country-rocks of the dykes; (G) microgranodiorite with enclaves from a dyke of the Tin Amali Dyke Swarm; (H) outcrop from the Ouhot Complex (Edembo Terrane) showing big granitic leucosomes within the migmatites.

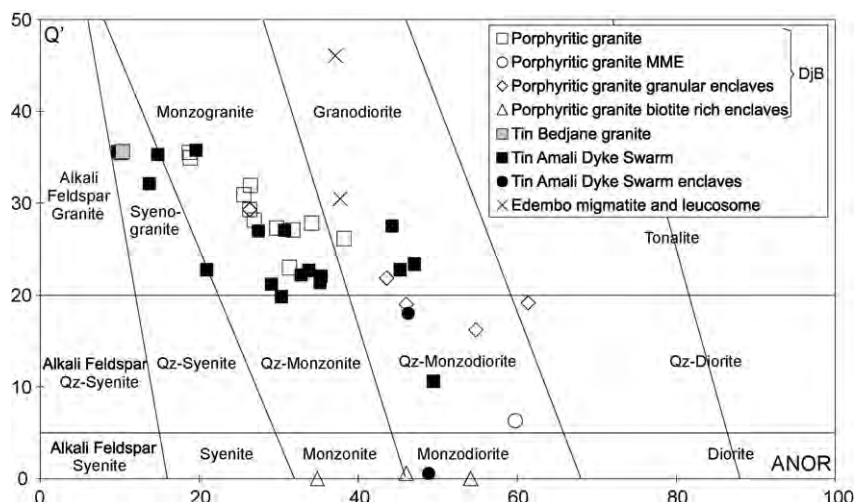


Fig. 3. Q'-Anor nomenclature diagram (values from CIPW norm) following Streckeisen and Le Maitre (1979). DjB = Djanet Batholith. Label axes on figure.

is subhorizontal and N160° oriented. As a whole, although a more detailed structural study is needed, the Edembo metamorphism and deformation occurred within a transpressive environment.

The Edembo Terrane also comprises granites and dykes such as the Mariaou and Tiska complexes. The dykes are oriented NW–SE, similar to the Tin Amali Dyke Swarm in the Djanet Terrane.

3. Zircon U–Pb geochronology

Detrital zircons have been dated by laser ablation ICP-MS at the University of Montpellier II, France and zircons from magmatic bodies by SHRIMP at Curtin University of Technology in Perth, Western Australia (Tables 1–3). Analytical techniques including results on standards are given in the appendix.

3.1. Djanet Group sediments

Fifty-nine detrital zircons from two samples of the Djanet Group have been analyzed (Table 1). Sample TOD47 is an arkosic sandstone and TOD45 a conglomerate. Forty-nine analyses with <8% discordance can therefore be used with confidence. Ages are reported based on ²⁰⁷Pb/²⁰⁶Pb (grains older than 1 Ga) or ²⁰⁶Pb/²³⁸U (grains younger than 1 Ga).

Seventeen zircons were analyzed from the arkosic sandstone TOD47. These display a bimodal zircon population (Fig. 4A and B) with a Neoproterozoic group (peaks at 595, 648 and 712 Ma) and a Palaeoproterozoic group (peaks at 1892 and 2014 Ma). The two youngest concordant zircons yield an age of 591 ± 10 Ma (#TOD47-1 and -15). Zircon #TOD47-15 alone gives a similar age of 589 ± 11 Ma (Fig. 4B, inset).

Forty-two detrital zircons were analyzed from the conglomerate TOD45 and this dataset displays a much wider range of ages but the age spectrum is still characterized by the absence of Mesoproterozoic zircons (Fig. 4C and D). Ages similar to those found in sandstone TOD47 are also present in the conglomerate: 602, 638, 673, 735 and 1908 Ma. The conglomerate also shows ages of 947, 1750, 2402, 2438, 2650, 2800, 2844 and 3232 Ma. The four youngest concordant zircons give a concordia age of 605 ± 4 Ma while the youngest analysis provides a concordia age of 597 ± 10 Ma (#TOD45-54; Fig. 4D, inset). These ages are slightly older, but within errors of the youngest zircons from sample TOD47 (591 ± 10 Ma and 589 ± 11 Ma). Combined, these results indicate that Djanet Group sediments were deposited after ~590 Ma.

3.2. Djanet Batholith

Eleven spots have been measured in cores and rims of zircons from the Djanet Batholith (sample TOD74, porphyritic granite; Table 2; Fig. 5A). Zircons have concentric zoning concordant with the external shape of the crystals (Fig. 5A). No age difference has been observed between cores and rims, indicating that both formed during crystallization of the batholith. Ten spots (excluding discordant spot #TOD74-1) define a discordia age of 573 ± 15 Ma (MSWD = 1.3; Fig. 5B), including two reversely discordant spots. Excluding these, the eight remaining spots define an indistinguishable age of 571 ± 16 Ma but with a much lower MSWD (0.41). Three spots yield a concordia age of 562 ± 3 Ma (MSWD of concordance = 0.23) although they appear slightly discordant. We thus consider conservatively that the best approximation of the Djanet Batholith crystallization age is given by the discordia line upper intercept of 571 ± 16 Ma. This age, within errors, can also be attributed to the greenschist-facies deformation that affected the Djanet Group as the Djanet batholith was affected at least by the vanishing deformation but still under greenschist ductile conditions.

3.3. Tin Bedjane Pluton

Fifteen zircons have been analyzed from two samples (TOD56 and TOD86; Table 2). Only two zircons were analyzed from TOD86 but these ages are indistinguishable from those of TOD56. Consequently, the two samples are considered together. Zircons display zoning concordant with their external shape; rare cores are curiously rounded (Fig. 5C). Cores, including rounded ones, and rims give the same ages, with the exception of one CL-bright crystal. Seven zircons are subconcordant and give an age of 568 ± 5 Ma (MSWD = 4.3; Fig. 5D) interpreted as dating crystallization of the Tin Bedjane Pluton. The CL-bright zircon (56.6) is concordant at 898 ± 17 Ma and is interpreted as an inherited grain. Two zircons (56.1 and 56.8r) are discordant but their ²⁰⁶Pb/²³⁸U ages are consistent with an age of 568 ± 5 Ma for the Tin Bedjane Pluton. This discordance can be interpreted either as because these zircons contain a small proportion of inherited lead or as a result of analytical uncertainty on the measurement of ²⁰⁷Pb. Because the analysis 56.8r is the rim of a zircon whose core (56.8c) is subconcordant at 568 ± 5 Ma, we favour the second interpretation.

We consider that the concordia age of 568 ± 5 Ma for the Tin Bedjane Pluton constitutes a minimum age constraint for deposition of the Djanet Group and probably also for its subsequent deformation

Table 1
U–Pb LA-ICP-MS data for the Djinet Group.

Spot name	ppm U	ppm Th	$^{232}\text{Th}/^{238}\text{U}$	ppm Rad ^{206}Pb	$^{207}\text{Pb}/^{206}\text{Pb}$	$1\sigma\%$ err	$^{207}\text{Pb}/^{235}\text{U}$	$1\sigma\%$ err	$^{206}\text{Pb}/^{238}\text{U}$	$1\sigma\%$ err	Err corr	Age	$^{207}\text{Pb}/^{206}\text{Pb}$	1σ err	%Disc
TOD47															
tod1	136	51	0.37	13.2	0.0598	0.58	0.821	3.13	0.0996	3.07	0.983	596	3.07	13	-2.5
tod2	677	409	0.60	251.4	0.1148	0.56	5.361	3.26	0.3386	3.21	0.985	1877	3.21	10	-0.1
tod3	136	51	0.37	13.2	0.1161	0.22	5.571	3.03	0.3481	3.02	0.997	1897	3.02	4	-1.5
tod4	542	496	0.92	62.4	0.0606	0.75	0.852	3.00	0.1019	2.90	0.968	625	2.90	16	-0.1
tod5	91	56	0.62	38.4	0.1235	1.03	6.323	1.93	0.3714	1.63	0.844	2007	1.63	18	-1.4
tod6	132	47	0.36	13.1	0.0610	0.63	0.834	2.25	0.0992	2.16	0.960	639	2.16	14	4.8
tod7	127	136	1.07	15.0	0.0628	1.20	0.851	1.43	0.0983	0.78	0.546	702	0.78	25	16.1
tod9	306	27	0.09	30.0	0.0593	0.29	0.834	3.74	0.1019	3.72	0.997	579	3.72	6	-7.5
tod11	288	152	0.53	34.2	0.0613	0.30	0.931	2.97	0.1101	2.95	0.995	650	2.95	7	-3.4
tod14	161	107	0.67	59.3	0.1160	0.25	5.289	3.74	0.3308	3.73	0.998	1895	3.73	5	2.9
tod15	187	196	1.04	18.7	0.0597	0.32	0.778	1.46	0.0945	1.42	0.975	594	1.42	7	2.1
tod16	404	243	0.60	156.4	0.1156	0.22	5.411	3.42	0.3395	3.42	0.998	1889	3.42	4	0.3
tod17	162	69	0.42	15.2	0.0620	0.69	0.807	3.29	0.0944	3.22	0.978	674	3.22	15	16.0
tod18	172	108	0.63	19.3	0.0631	0.68	0.945	1.75	0.1087	1.61	0.922	710	1.61	14	6.7
tod19	1163	326	0.28	131.4	0.0661	0.37	0.981	3.15	0.1075	3.13	0.993	810	3.13	8	23.1
tod21	1247	340	0.27	116.9	0.0677	0.85	0.843	1.21	0.0902	0.86	0.710	861	0.86	18	54.6
tod23	177	143	0.81	69.6	0.1165	0.26	5.431	2.15	0.3381	2.13	0.993	1903	2.13	5	1.4
TOD45															
tod24	241	149	0.62	26.6	0.0603	0.77	0.887	4.12	0.1067	4.05	0.982	614	4.05	17	-6.0
tod25	94	72	0.77	74.7	0.2570	0.44	23.523	2.41	0.6638	2.37	0.983	3228	2.37	7	-1.6
tod26	152	142	0.93	18.1	0.0600	1.03	0.861	1.08	0.1040	0.32	0.297	604	0.32	22	-5.3
tod27	422	173	0.41	56.7	0.0641	0.97	1.121	2.23	0.1268	2.00	0.900	745	2.00	20	-3.2
tod28	91	44	0.48	59.6	0.2020	0.47	15.506	0.54	0.5568	0.27	0.499	2842	0.27	8	-0.4
tod29	232	83	0.36	23.4	0.0603	0.88	0.821	2.18	0.0987	1.99	0.916	615	1.99	19	1.4
tod30	155	85	0.55	18.0	0.0615	1.91	0.944	1.94	0.1113	0.33	0.169	656	0.33	41	-3.5
tod31	61	47	0.77	7.6	0.0647	0.97	0.960	1.14	0.1076	0.59	0.521	765	0.59	20	16.2
tod32	132	97	0.74	14.3	0.0610	0.23	0.812	2.09	0.0965	2.08	0.994	639	2.08	5	7.5
tod33	76	30	0.39	8.2	0.0597	1.73	0.846	1.76	0.1027	0.35	0.196	593	0.35	37	-6.0
tod34	583	266	0.46	65.5	0.0605	0.50	0.870	2.51	0.1044	2.46	0.980	620	2.46	11	-3.1
tod35	137	39	0.28	15.0	0.0623	1.26	0.950	2.57	0.1106	2.24	0.871	683	2.24	27	1.0
tod36	343	67	0.20	34.6	0.0599	0.24	0.830	3.57	0.1005	3.56	0.998	599	3.56	5	-2.9
tod37	121	80	0.66	15.5	0.0639	0.42	1.039	4.24	0.1180	4.21	0.995	737	4.21	9	2.5
tod38	92	49	0.53	62.4	0.1791	0.76	11.938	1.55	0.4834	1.35	0.870	2645	1.35	13	4.0
tod39	149	51	0.34	16.4	0.0600	1.81	0.905	2.23	0.1093	1.30	0.582	604	1.30	39	-9.7
tod40	143	64	0.45	15.4	0.0608	0.85	0.850	5.67	0.1014	5.61	0.989	632	5.61	18	1.4
tod41	228	106	0.46	88.3	0.1170	0.26	5.574	1.65	0.3456	1.63	0.988	1910	1.63	5	-0.2
tod42	124	52	0.42	21.1	0.0707	0.69	1.534	4.04	0.1574	3.98	0.985	949	3.98	14	0.8
tod43	69	101	1.47	30.8	0.1081	0.53	4.833	2.97	0.3243	2.92	0.984	1768	2.92	10	-2.4
tod44	573	112	0.19	63.5	0.0608	0.34	0.916	2.80	0.1093	2.78	0.992	632	2.78	7	-5.5
tod45	256	199	0.78	152.4	0.1582	0.23	9.828	1.43	0.4504	1.41	0.987	2437	1.41	4	1.7
tod46	258	110	0.43	131.0	0.1547	0.56	9.592	2.73	0.4496	2.67	0.978	2399	2.67	10	0.2
tod47	98	65	0.66	111.5	0.0618	1.62	0.935	2.72	0.1098	2.18	0.803	666	2.18	35	-0.7
tod48	257	144	0.56	32.6	0.0622	0.41	1.055	1.74	0.1230	1.69	0.971	681	1.69	9	-9.0
tod49	269	7	0.03	159.3	0.1964	0.52	14.720	2.39	0.5436	2.33	0.976	2796	2.33	8	-0.1
tod50	79	68	0.86	29.4	0.1071	0.40	4.793	2.44	0.3245	2.41	0.986	1751	2.41	7	-3.3
tod51	444	153	0.35	49.1	0.0609	0.43	0.918	2.11	0.1094	2.06	0.979	635	2.06	9	-5.2
tod52	259	107	0.41	33.3	0.0632	0.56	1.071	1.10	0.1229	0.95	0.862	715	0.95	12	-4.3
tod53	329	113	0.34	35.8	0.0607	0.76	0.889	3.39	0.1062	3.31	0.975	630	3.31	16	-3.2
tod54	270	164	0.61	28.7	0.0603	0.82	0.804	1.23	0.0968	0.91	0.742	613	0.91	18	2.9
tod55	979	44	0.04	90.9	0.0585	0.40	0.794	1.63	0.0983	1.58	0.969	550	1.58	9	-9.1

Table 1 (Continued)

Spot name	ppm U	ppm Th	²³² Th/ ²³⁸ U	ppm Rad ²⁰⁶ Pb	²⁰⁷ Pb/ ²⁰⁶ Pb _r	1σ% err	²⁰⁷ Pb/ ²³⁵ U	1σ% err	²⁰⁶ Pb/ ²³⁸ U	1σ% err	E _{irr} corr	²⁰⁷ Pb/ ²⁰⁶ Pb Age	1σ err	%Disc
tod56	401	152	0.38	199.7	0.1603	0.62	10.049	1.57	0.4546	1.45	0.920	2459	10	1.8
tod57	1008	270	0.27	106.7	0.0594	0.86	0.873	2.72	0.1067	2.58	0.949	581	19	-11.1
tod58	101	38	0.37	110	0.0601	0.77	0.883	0.91	0.1066	0.49	0.537	608	17	-6.9
tod59	448	138	0.31	65.5	0.0660	0.42	1.329	2.02	0.1460	1.98	0.979	807	9	-8.1
tod60	67	26	0.40	7.1	0.0600	1.12	0.857	1.32	0.1037	0.71	0.534	603	24	-5.3
tod61	358	357	1.00	41.2	0.0598	0.36	0.817	0.59	0.0991	0.46	0.786	596	8	-2.1
tod62	151	147	0.97	18.5	0.0599	0.71	0.841	2.49	0.1018	2.39	0.959	600	15	-4.1
tod63	497	288	0.58	58.4	0.0619	0.69	0.940	0.92	0.1101	0.62	0.670	672	15	-0.2
tod64	64	14	0.22	6.6	0.0619	0.51	0.903	0.73	0.1057	0.52	0.711	672	11	3.8
tod65	80	28	0.35	8.2	0.0615	1.02	0.851	2.03	0.1004	1.75	0.864	656	22	6.4

under greenschist-facies conditions although a subcontemporaneity cannot be excluded.

3.4. Tin Amali Dyke Swarm

Fourteen zircons have been analyzed from sample TOD59 taken from a rhyolitic dyke belonging to the Tin Amali Dyke Swarm (Table 2). Crystals show zoning concordant with the external crystal, rarely discordant. Rims are generally thin (Fig. 5E). However three spots were obtained on sufficiently large (oscillatory-zoned) rims (Fig. 5E) which gave a concordia age of 558 ± 6 Ma (MSWD = 1.5; Fig. 5F), which we consider to best approximate of the emplacement age of the Tin Amali Dyke Swarm. This age corresponds also to the brittle deformation that occurred during the emplacement of the dyke swarm.

Five cores define a concordia age of 570 ± 6 Ma (MSWD = 5.5; Fig. 5F), identical to that of the Djanet Batholith (571 ± 16 Ma) from which they may have been derived. Other inherited cores are present in this sample: two spots define a concordia age of 629 ± 9 Ma (MSWD = 1.5); two spots give $^{206}\text{Pb}/^{238}\text{U}$ ages of 735 ± 13 Ma and 865 ± 24 Ma but are reversely discordant (Fig. 5F, upper inset); and one discordant zircon gives a $^{207}\text{Pb}/^{206}\text{Pb}$ age of 2091 ± 40 Ma (Fig. 5F, lower inset).

3.5. Migmatites and associated granite from the Edembo Terrane

Fourteen zircons from migmatitic gneiss sample TOD67 belonging to the Ouhot Complex (Edembo Terrane) have been analyzed (Table 3). In cathodo-luminescence (CL) images, zircons display large rounded cores surrounded by thin rims (Fig. 6A). Rims are too thin to be dated. The nine youngest cores plot near concordia, between 675 ± 15 and 596 ± 10 Ma (Fig. 6B). Rounded cores and this age range suggest that the protolith of this rock is of sedimentary origin. Other cores gave older ages: one strongly zoned core gave a concordant age of 832 ± 13 Ma; three CL-bright cores are concordant giving a well-constrained age of 1831 ± 16 Ma (MSWD of concordance = 0.30) and one discordant zoned core indicates a minimum Archaean age of 2940 ± 17 Ma ($^{207}\text{Pb}/^{206}\text{Pb}$ age). The youngest age (596 ± 10 Ma) is thus a maximum age for the age of the migmatitization, from which the younger undated rims probably resulted.

In order to constrain the age of the migmatitization, we analyzed zircons from a thick granitic leucosome within the Ouhot migmatites (Fig. 2H; sample TOD69; Fig. 6C). Its complex shape, its small volume and connectivity with migmatitic parts of the gneiss indicate that it formed about the same time as the migmatites. Zircons from this sample display cores in CL-images but the internal structures of these cores are generally concordant with that of the external crystal suggesting a penecontemporaneous magmatic origin. However, some crystals display xenomorphic or rounded cores (Fig. 6C). Twenty-six zircons from the Ouhot leucosome were analyzed. Thirteen concordant spots from cores and rims define an age of 568 ± 4 Ma (Fig. 6D). Inherited zircons are also recorded: three concordant spots give an age of 620 ± 6 Ma. Finally one xenomorphic core is strongly discordant but gives a Palaeoproterozoic age of 1863 ± 73 Ma if the discordia is forced through 568 Ma. In addition, nine zircons have suffered some Pb-loss, spreading out along a present-day Pb-loss trend, and do not give useful ages. The best age estimate for formation of the granitic leucosome coeval to the migmatitization is thus 568 ± 4 Ma, which is identical to the Tin Bedjane Pluton age (568 ± 5 Ma) from the Djanet Terrane.

3.6. Zircon U–Pb geochronology summary

Deposition and greenschist-facies metamorphism of the Djanet Group occurred between 590 ± 10 Ma (age of the youngest detri-

Table 2
U–Pb SHRIMP data for porphyritic granite of the Djanet Batholith, Tin Bedjane Pluton and Tin Anjali Dyke Swarm.

Spot name	% comm ²⁰⁶ Pb	ppm U	ppm Th	²³² Th/ ²³⁸ U	ppm Rad ²⁰⁶ Pb	²⁰⁷ Pb/ ²⁰⁶ Pb	1σ% err	²⁰⁷ Pb/ ²³⁵ U	1σ% err	²⁰⁶ Pb/ ²³⁸ U	1σ% err	Err corr	²⁰⁶ Pb/ ²³⁸ U Age	1σ% err
Djanet Batholith (sample: TOD74)														
tod74-1	1.55	1124	288	0.26	88.1	0.0745	1.00	0.767	2.50	0.0898	0.33	0.133	552	2
tod74-2	0.10	227	127	0.58	17.9	0.0606	1.19	0.756	1.65	0.0916	0.66	0.400	565	4
tod74-3	0.07	1008	329	0.34	78.8	0.0596	0.56	0.740	0.67	0.0909	0.31	0.466	561	2
tod74-4	0.20	1127	352	0.32	87.2	0.0610	0.64	0.736	1.19	0.0899	0.30	0.255	554	2
tod74-5c	2.61	425	156	0.38	27.4	0.0796	0.84	0.590	4.65	0.0731	0.59	0.127	454	2
tod74-5r	0.55	1556	325	0.22	96.8	0.0645	0.49	0.597	1.23	0.0720	0.28	0.227	446	1
tod74-6c	0.20	236	102	0.45	18.7	0.0591	1.18	0.730	1.75	0.0923	0.67	0.380	570	4
tod74-6r	0.10	1244	287	0.24	89.3	0.0603	0.84	0.685	1.42	0.0835	1.04	0.736	516	5
tod74-7	0.19	713	349	0.51	54.6	0.0602	0.67	0.720	1.19	0.0890	0.41	0.340	549	2
tod74-8c	0.83	156	108	0.72	12.3	0.0616	1.39	0.687	4.23	0.0910	0.81	0.192	564	4
tod74-9	0.17	784	163	0.22	61.5	0.0610	0.62	0.749	1.18	0.0911	0.50	0.428	562	3
Tin Bedjane Massif (samples: TOD56 and TOD86)														
tod56-1	-0.10	266	104	0.40	21.5	0.0599	1.12	0.789	1.42	0.0942	0.62	0.436	579	4
tod56-2	0.89	353	248	0.73	26.0	0.0682	1.39	0.713	2.94	0.0848	0.57	0.194	522	3
tod56-3	0.23	322	127	0.41	25.3	0.0615	1.01	0.750	1.86	0.0913	0.83	0.446	563	5
tod56-4	0.14	444	234	0.54	34.8	0.0604	0.92	0.745	1.42	0.0911	0.49	0.345	562	3
tod56-5	0.47	732	124	0.17	56.5	0.0631	0.80	0.730	2.07	0.0894	0.63	0.305	552	3
tod56-6	0.53	85	66	0.80	11.0	0.0740	1.43	1.434	3.12	0.1494	1.01	0.324	897	9
tod56-7	0.54	244	45	0.19	18.6	0.0631	1.17	0.715	2.66	0.0884	0.67	0.253	546	4
tod56-8c	0.28	56	28	0.53	4.4	0.0622	2.48	0.753	7.52	0.0911	1.48	0.197	561	8
tod56-8r	-0.21	260	69	0.27	20.5	0.0608	1.13	0.792	1.27	0.0918	0.62	0.489	564	3
tod56-9	0.00	3295	1110	0.35	258.6	0.0596	0.32	0.913	0.91	0.0913	0.85	0.929	563	5
tod56-10	0.49	428	191	0.46	26.1	0.0652	0.92	0.596	2.29	0.0706	0.57	0.249	437	2
tod56-11	1.03	844	388	0.47	65.6	0.0676	0.61	0.731	2.64	0.0896	0.40	0.150	553	2
tod56-12	0.15	279	96	0.35	22.3	0.0590	1.09	0.738	2.17	0.0927	0.66	0.307	572	4
tod86-1	0.36	229	95	0.43	18.4	0.0615	1.34	0.752	3.59	0.0930	0.97	0.271	574	5
tod86-2	0.23	891	528	0.61	72.0	0.0599	0.69	0.750	1.37	0.0938	0.69	0.504	579	4
Tin Anjali Dyke Swarm (sample: TOD59)														
tod59-1	0.51	334	233	0.72	29.7	0.0632	1.04	0.838	2.73	0.1029	0.85	0.310	633	5
tod59-2	0.35	297	153	0.53	23.2	0.0598	1.19	0.710	2.61	0.0905	0.88	0.338	560	5
tod59-3	0.76	131	96	0.76	10.1	0.0596	1.81	0.660	8.51	0.0894	1.26	0.148	556	6
tod59-4	0.79	340	312	0.95	27.0	0.0597	1.38	0.675	4.21	0.0918	0.88	0.210	570	5
tod59-5	2.41	69	57	0.85	8.7	0.0808	1.75	1.210	8.96	0.1436	1.48	0.165	872	11
tod59-6	1.44	146	114	0.81	12.9	0.0621	2.40	0.705	19.41	0.1010	1.82	0.094	628	8
tod59-7	0.23	755	400	0.55	60.2	0.0588	0.79	0.727	1.51	0.0927	0.71	0.473	573	4
tod59-8	2.56	82	156	1.97	8.1	0.0614	3.66	0.640	21.13	0.1130	2.24	0.106	709	14
tod59-9	0.30	280	179	0.66	22.2	0.0595	1.26	0.725	3.38	0.0922	0.92	0.272	570	5
tod59-10	0.17	515	238	0.48	41.1	0.0603	0.91	0.753	1.73	0.0927	0.76	0.440	572	4
tod59-11c	1.06	235	41	0.18	69.1	0.1388	0.52	6.049	1.41	0.3389	0.84	0.596	1852	15
tod59-12	1.08	420	134	0.33	33.1	0.0679	0.97	0.740	3.45	0.0908	0.83	0.242	560	4
tod59-13	0.42	275	77	0.29	28.5	0.0636	1.09	0.988	2.97	0.1202	0.94	0.317	735	7
tod59-14	0.07	603	339	0.58	48.3	0.0597	0.84	0.761	1.37	0.0933	0.74	0.537	575	4

Table 3
U–Pb SHRIMP data for the Edebo granite and migmatite.

Spot name	% comm ²⁰⁶ Pb	ppm U	ppm Th	²³² Th/ ²³⁸ U	ppm Rad ²⁰⁶ Pb	²⁰⁷ Pb/ ²⁰⁶ Pb	1σ% err	²⁰⁷ Pb/ ²³⁵ U	1σ% err	²⁰⁶ Pb/ ²³⁸ U	1σ% err	Err corr	²⁰⁶ Pb/ ²³⁸ U Age	1σ% err
Edebo migmatite (sample: TOD67)														
tod67-1	0.23	78	69	0.92	22.1	0.1146	0.82	5.111	1.67	0.3292	1.06	0.636	1834	19
tod67-2	0.27	263	52	0.20	22.4	0.0605	1.36	0.796	2.47	0.0990	0.85	0.346	610	5
tod67-3	0.08	289	144	0.51	72.2	0.1126	0.44	4.481	0.92	0.2903	0.77	0.837	1623	12
tod67-4	0.42	133	177	1.37	11.6	0.0611	1.41	0.799	3.58	0.1005	1.04	0.290	619	6
tod67-5	0.32	43	47	1.12	12.6	0.1133	1.51	5.180	2.35	0.3398	1.28	0.546	1896	24
tod67-6	1.77	54	26	0.50	4.9	0.0664	2.11	0.757	9.99	0.1052	1.52	0.152	652	9
tod67-7	0.20	190	89	0.49	22.6	0.0675	0.96	1.254	1.77	0.1381	0.88	0.499	835	7
tod67-8	1.26	68	64	0.97	6.3	0.0637	1.89	0.787	8.86	0.1067	1.36	0.154	660	8
tod67-9	0.12	765	225	0.30	67.9	0.0605	0.59	0.847	1.05	0.1032	0.71	0.676	634	4
tod67-10	-0.01	332	220	0.69	30.1	0.0623	0.88	0.908	1.22	0.1056	0.84	0.687	646	5
tod67-11	0.56	120	78	0.67	11.4	0.0630	1.86	0.885	7.28	0.1099	1.28	0.176	675	8
tod67-12	0.50	236	192	0.84	19.7	0.0611	1.07	0.759	2.47	0.0966	0.88	0.355	596	5
tod67-13	0.02	156	80	0.53	72.1	0.2148	0.55	15.932	1.00	0.5385	0.84	0.835	2706	26
tod67-14	0.12	876	501	0.59	79.8	0.0621	0.53	0.893	1.01	0.1059	0.70	0.692	649	4
Edebo granite (sample: TOD69)														
tod69-1r	0.86	545	24	0.05	41.1	0.0571	2.25	0.685	2.36	0.0870	0.73	0.309	538	4
tod69-2r	0.94	1185	70	0.06	86.2	0.0592	1.79	0.684	1.91	0.0838	0.65	0.343	519	3
tod69-3c	0.55	205	82	0.41	16.3	0.0553	3.03	0.704	3.17	0.0923	0.94	0.295	569	5
tod69-4c	0.55	592	298	0.52	47.8	0.0589	1.81	0.759	1.95	0.0934	0.72	0.370	576	4
tod69-5c	2.09	278	39	0.15	21.4	0.0618	4.56	0.748	4.64	0.0877	0.86	0.186	542	4
tod69-6r	0.46	641	36	0.06	50.9	0.0606	1.97	0.768	2.12	0.0920	0.78	0.368	567	4
tod69-7-2	0.04	707	116	0.17	57.2	0.0597	0.84	0.775	1.54	0.0941	1.29	0.836	580	7
tod69-7c	0.40	67	34	0.53	5.3	0.0586	5.27	0.741	5.44	0.0916	1.36	0.250	565	7
tod69-8r	1.50	841	493	0.61	74.1	0.0593	2.34	0.826	2.44	0.1010	0.67	0.277	620	4
tod69-9c	0.17	139	57	0.42	25.4	0.1019	1.35	2.980	1.84	0.2122	1.25	0.678	1240	14
tod69-9r	0.22	520	11	0.02	41.4	0.0580	1.24	0.740	1.44	0.0924	0.72	0.503	570	4
tod69-10-2	0.32	833	27	0.03	66.9	0.0591	1.15	0.758	1.64	0.0931	1.17	0.714	574	6
tod69-10-3	0.65	1734	204	0.12	119.5	0.0593	1.15	0.651	1.65	0.0797	1.18	0.715	494	6
tod69-10c	1.46	214	72	0.35	17.0	0.0543	4.77	0.682	4.86	0.0912	0.94	0.193	562	5
tod69-11-1	0.07	568	222	0.40	49.0	0.0609	1.13	0.842	1.66	0.1003	1.21	0.729	616	7
tod69-11c	-0.01	442	330	0.77	38.3	0.0618	1.09	0.858	1.32	0.1007	0.74	0.563	619	4
tod69-11c	0.29	438	243	0.57	37.3	0.0576	1.62	0.786	1.81	0.0990	0.80	0.444	608	5
tod69-12-2	0.11	1147	246	0.22	88.9	0.0580	0.76	0.720	1.38	0.0901	1.15	0.834	556	6
tod69-12-3	0.63	1222	295	0.25	96.1	0.0601	1.19	0.754	1.66	0.0909	1.15	0.695	561	6
tod69-12c+r	0.29	226	57	0.26	16.6	0.0573	1.74	0.671	1.94	0.0850	0.87	0.447	526	4
tod69-13c	0.97	82	45	0.57	6.7	0.0566	4.94	0.736	5.09	0.0943	1.23	0.241	581	7
tod69-14-1	0.06	2836	226	0.08	181.2	0.0590	0.48	0.605	1.23	0.0743	1.14	0.923	462	5
tod69-16-1	0.16	431	18	0.04	34.3	0.0591	2.04	0.756	2.36	0.0927	1.20	0.505	572	7
tod69-16-2	0.04	650	16	0.02	53.3	0.0616	0.86	0.810	1.17	0.0954	1.17	0.805	587	7
tod69-20-1	1.09	1016	73	0.07	75.2	0.0571	1.91	0.671	2.24	0.0852	1.16	0.519	527	6
tod69-23-1	2.10	880	82	0.10	69.1	0.0595	3.52	0.734	3.72	0.0894	1.21	0.324	552	6

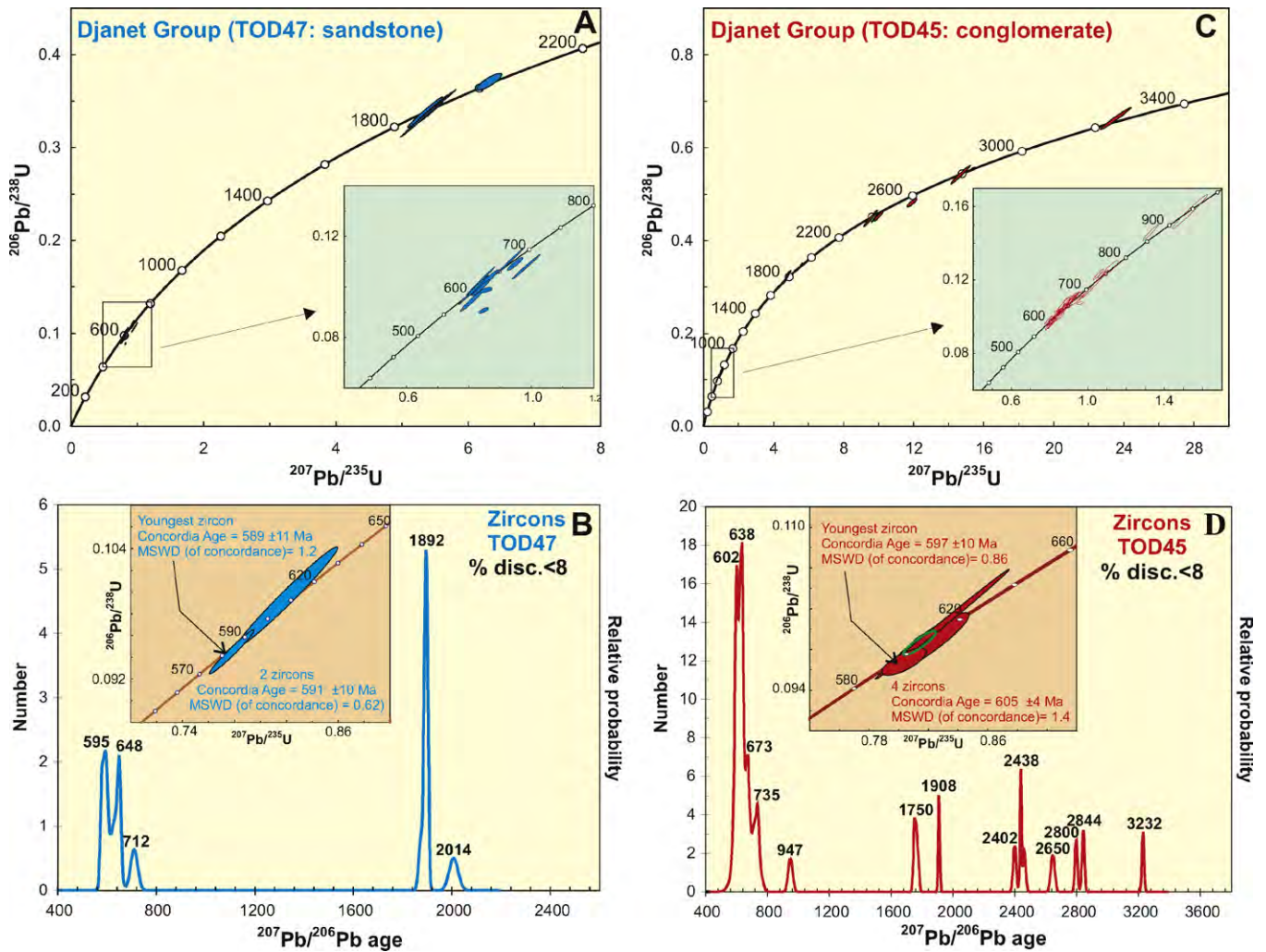


Fig. 4. U–Pb concordia diagrams (A and C) and age spectra (B and D) for the Djanet Group (samples TOD45 and TOD47) with, as inset in C and D, the concordia age of the youngest zircons in each sample.

tal zircons) and 571 ± 16 Ma (the age of Djanet Batholith, which is syn- or late-metamorphic) or 568 ± 5 Ma (the age of the intruding Tin Bedjane Pluton higher in the crust). Metamorphism was probably at least partly induced by heat from the Djanet Batholith; the relatively large error on the age of the Djanet Batholith most likely encompass the age of the greenschist-facies metamorphism. The source of the Djanet Group comprises rocks with a large range of ages, from 595 Ma to 3.25 Ga with no Mesoproterozoic ages, which is typical of West Africa and the Tuareg Shield (Caby and Andreopoulos-Renaud, 1987; Liégeois et al., 1994, 2003; Peucat et al., 2003). Indeed, late Archaean ages (2650 Ma) may have been derived from Archaean granulitic basement in the Gour Oumelalen area, NE LATEA (Peucat et al., 2003). Ages of 1750 Ma are known in the western Tuareg Shield (Caby and Andreopoulos-Renaud, 1983) and the Early Palaeoproterozoic and Archaean grains with ages of c. 2450, 2800, 3200 Ma, can have been supplied by erosion of the In Ouzzal terrane (Ouzegane et al., 2003 and references therein). Ages of c. 950 Ma, recorded in the Djanet Group and in the Tin Bedjane Pluton as inherited grains, are currently unknown in the Tuareg Shield, but continental rocks of 920–900 Ma have recently been dated to the east in the Bayuda desert of Sudan (Bayudian episode; Küster et al., 2008). Formerly, these ages were known only from detrital zircons (Avigad et al., 2005, 2007). The variety of detrital zircon ages suggests a complex provenance for

Djanet Group sediments that include a proximal, relatively immature source (presence of feldspar) as well as material from a wider, mature distribution system (large set of detrital zircon ages typical of the Tuareg Shield).

The Djanet Group was successively intruded by the Djanet Batholith (571 ± 16 Ma), the Tin Bedjane Pluton (568 ± 5 Ma) and the Tin Amali Dyke Swarm (558 ± 6 Ma). This indicates a relatively short magmatic event that lasted between 10 and 15 m.y. The age of this magmatic suite corresponds also to the age of the greenschist-facies metamorphism that affects the Djanet Group.

Ages of inherited zircon cores, taking into account the errors, coincide with ages in the Djanet Group detrital zircons. This suggests that these cores are inherited from melted Djanet Group sediments, or assimilated during ascent and emplacement of the magma. This is especially the case for the Tin Amali rhyolites.

Similar ages have been found in the neighbouring amphibolite-facies Edembo Terrane. Inherited zircons of detrital origin (metasediment TOD67) have ages ranging from 596 Ma to 2.94 Ga but with no Mesoproterozoic ages, deriving from the protolith of the Ouhot migmatite. Considering the similarity of this inherited zircon age signature with that of the Djanet Group, we suggest that the Ouhot migmatite is an amphibolite-facies equivalent of the latter. This proposition must be tested further, however. Whatever,

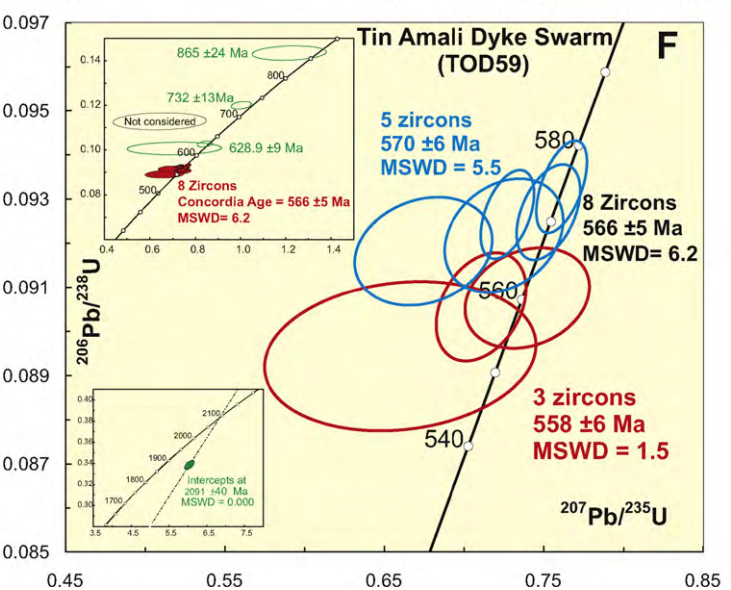
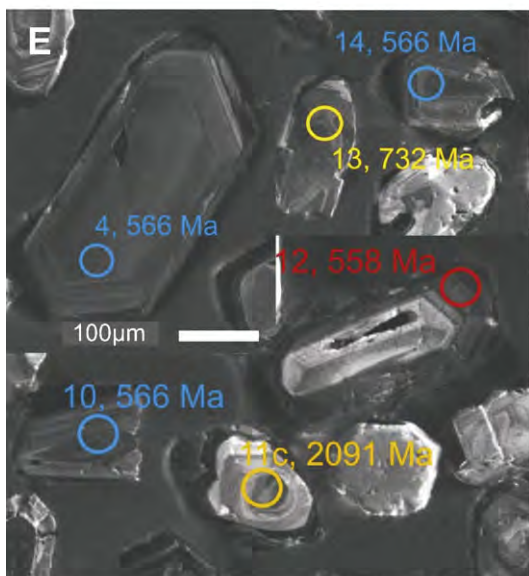
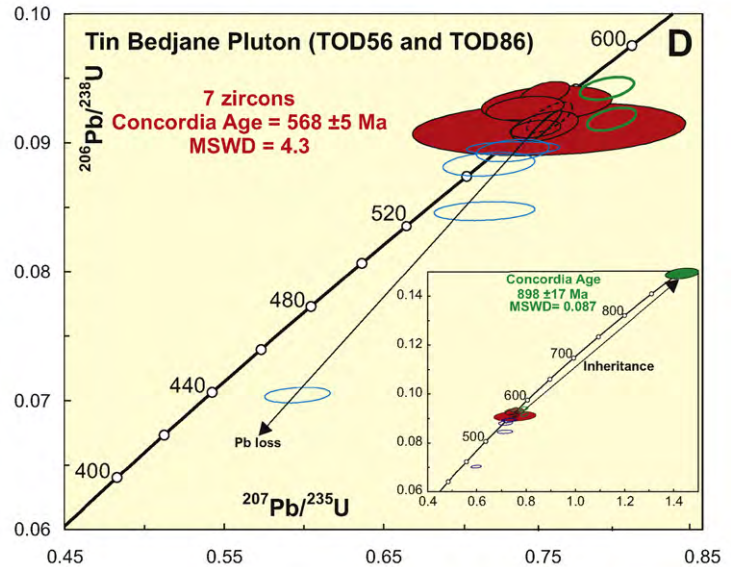
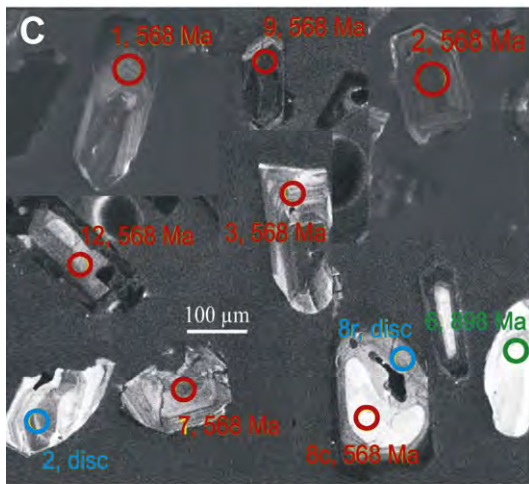
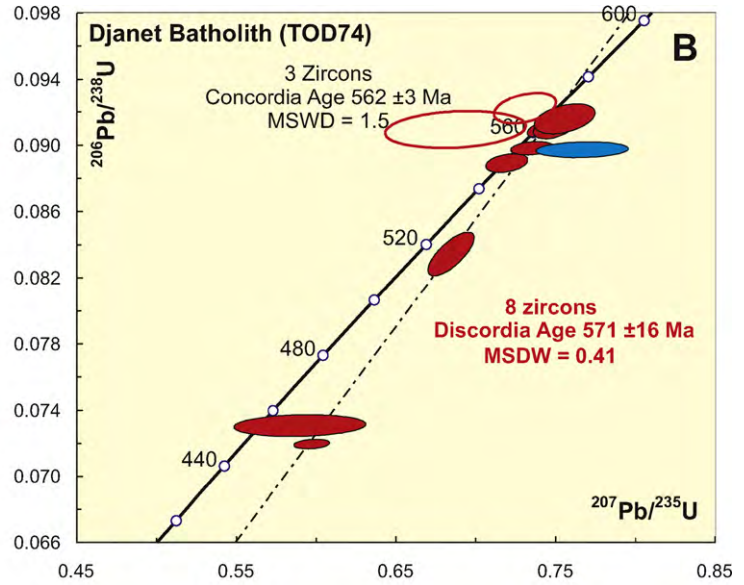
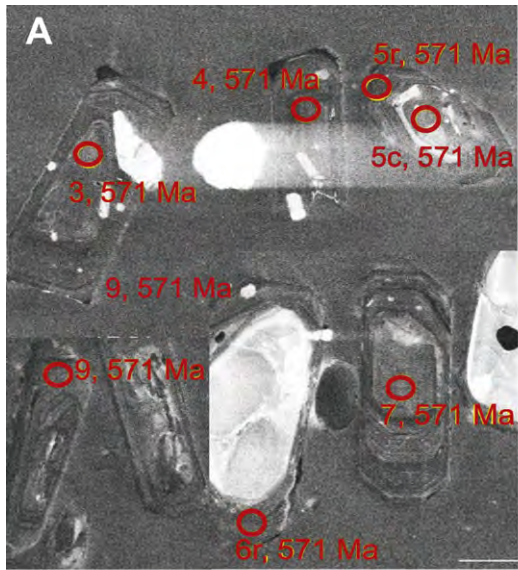


Fig. 5. Cathodo-luminescence images with dated spots and U–Pb concordia diagrams, respectively, for Djanet Batholith (sample TOD74; A and B); Tin Bedjane Pluton (samples TOD56 and TOD86; C and D) and Tin Amali Dyke Swarm (sample TOD59; E and F).

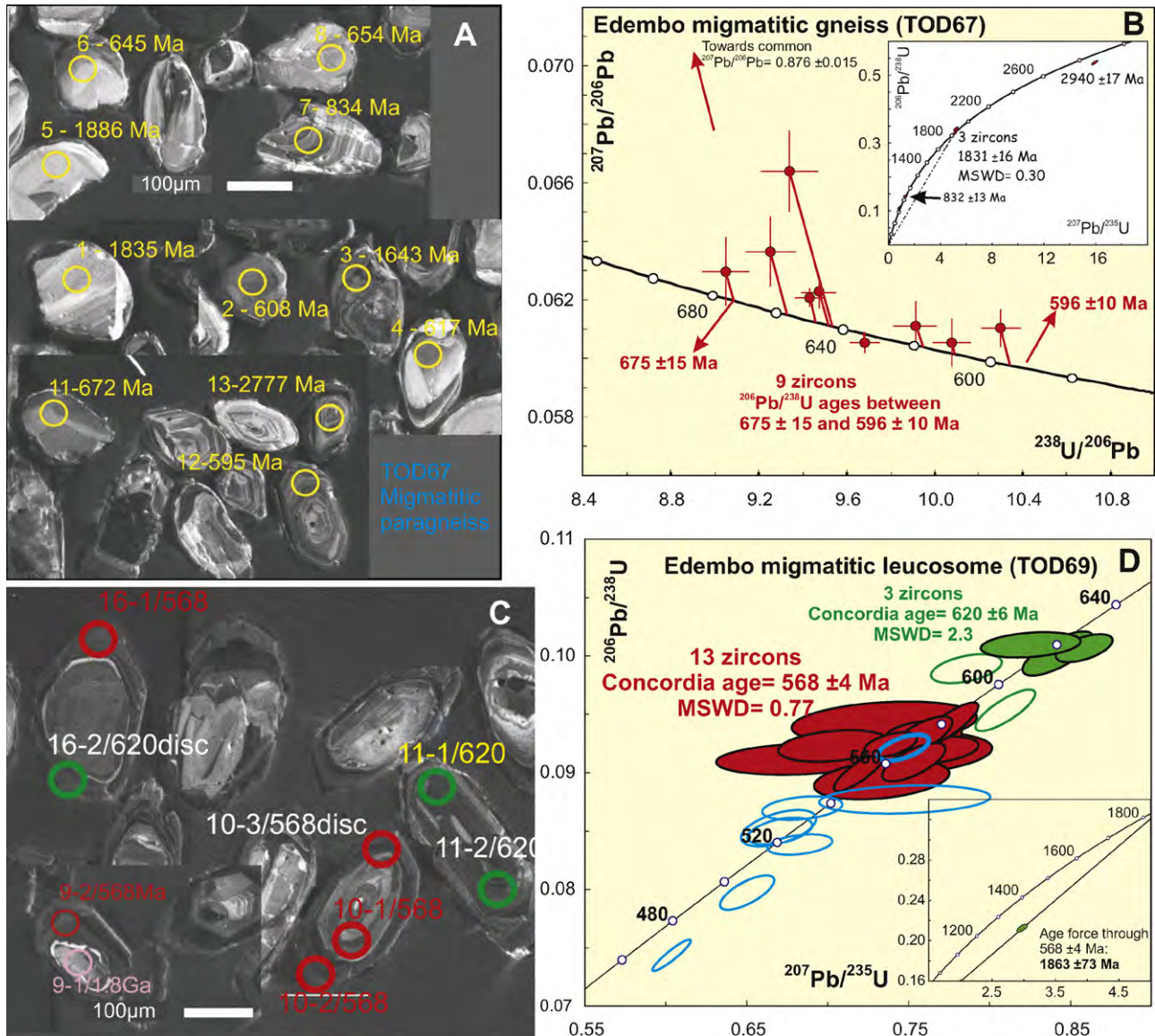


Fig. 6. Cathodo-luminescence images with dated spots and U–Pb concordia diagrams, respectively, for Edembo migmatite (sample TOD67; A and B) and Edembo migmatitic big leucosome (sample TOD69; C and D).

amphibolite-facies metamorphism and migmatitization occurred at 568 ± 4 Ma.

Thus, it is concluded that emplacement of the Djanet Batholith in the Djanet Terran, the greenschist metamorphism in the Djanet Terrane and the migmatitic metamorphism in the Edembo Terrane occurred during the same period of time.

4. Major and trace element geochemistry

Major and trace elements (Table 4) have been measured on 5 metasedimentary rocks and 2 associated mafic and felsic dykes from the Djanet Group, 12 granitoids and 10 enclaves from the Djanet Batholith, 2 granites from the Tin Bedjane Pluton, 17 rocks and 2 enclaves from the Tin Amali Dyke Swarm. In addition, analysis of the samples from the Ouhot migmatite and the Ouhot leucosome (Edembo Terrane) from which U–Pb zircon data were obtained, are provided. Major elements were determined by ICP-AES and trace elements by ICP-MS in the Geochemical Laboratory of the Royal Museum for Central Africa in Tervuren (see Liégeois et al., 2003 for analytical procedures).

4.1. The Djanet Group

Despite different grain sizes (TOD45 is conglomeratic, TOD47 is psammitic, the others are pelitic), the composition of Djanet Group sediments is rather homogeneous, in agreement with their uniform mineralogy. The rocks have 67–72% SiO_2 and are peraluminous (A/CNK from 1.12 to 1.21). Using chemical discrimination diagrams applied to sedimentary rocks (Bathia, 1983; Roser and Korsch, 1986), Djanet Group samples always fall in the continental arc or active continental margin fields (Fig. 7A–D). This implies efficient mixing during the sedimentation from a provenance that is dominated by immature continental arc inputs.

Major element homogeneity is mirrored in the trace elements which show very similar spidergrams and REE patterns (Fig. 8A and B). Djanet Group REE patterns are very similar to the average North American Shale Composite (NASC; Fig. 8A). NASC has a REE pattern similar to granites, especially the Peninsular Range Batholith (Gromet et al., 1984), in agreement with an active continental margin source type. Looking at the other element abundances (Fig. 8B), differences arise with the NASC reference, especially for the major

Table 4
Whole rock geochemistry (major and trace elements) for Djanet Batholith, Tin Bedjane Pluton, Tin Amali Dyke Swarm, Djanet Group and granite and migmatite from the Edembo Terrane.

Djanet Batholith		Granular enclaves										Biotite-rich enclaves				Xenolith								
Type	Monzogranite	Granodiorite					MME					Granular enclaves				Biotite-rich enclaves				Xenolith				
Sample	TOD53	TOD74	J6	J4	J19	DJ1	DJ6	DJ10	J9	J21	J18	J8	DJ7	MME	DJ8a	J7e	DJ8c	DJ2	DJ5	J8e	TOD73	DJ8b	J11	J11
SiO ₂	68.26	65.03	70.78	74.75	74.21	69.60	67.49	67.57	69.90	72.05	72.70	68.27	56.66	60.94	61.33	62.04	63.79	69.95	69.95	55.66	55.02	47.55	47.07	72.07
TiO ₂	0.43	0.51	0.24	0.14	0.16	0.31	0.49	0.53	0.33	0.33	0.31	0.38	1.01	0.91	0.67	0.82	0.75	0.31	0.31	0.95	1.23	2.32	2.32	0.47
Al ₂ O ₃	14.73	17.20	14.88	13.06	13.26	14.25	15.44	14.49	15.08	13.89	13.73	15.33	17.51	16.31	17.24	16.15	16.01	14.32	14.32	17.76	19.53	18.18	18.18	12.49
Fe ₂ O ₃ t	3.96	3.56	2.65	1.61	2.04	2.85	4.39	4.16	3.35	3.11	2.82	3.38	8.09	7.69	6.64	5.83	5.83	4.86	2.86	9.60	8.18	13.77	4.87	4.07
MnO	0.05	0.07	0.05	0.03	0.03	0.04	0.06	0.06	0.05	0.06	0.05	0.05	0.14	0.12	0.12	0.09	0.08	0.04	0.04	0.22	0.11	0.19	0.19	0.07
MgO	0.86	1.05	0.40	0.26	0.27	0.62	1.26	1.15	0.56	0.56	0.65	0.99	3.16	2.46	2.17	2.30	1.62	0.62	0.62	2.69	2.23	4.09	1.28	1.28
CaO	2.45	2.72	1.89	1.34	1.38	2.06	3.06	2.55	2.34	1.94	1.92	2.87	6.45	4.87	4.04	4.34	3.27	2.07	3.96	4.68	3.97	2.03	2.03	3.46
Na ₂ O	3.60	3.23	4.04	3.33	3.30	3.36	3.69	3.40	3.75	3.60	3.69	3.77	4.17	3.68	4.32	3.26	3.83	3.38	5.02	5.11	3.77	3.77	3.46	3.46
K ₂ O	4.04	4.74	4.13	4.64	4.76	4.55	3.55	4.19	4.31	4.36	4.11	3.74	2.47	2.26	2.55	3.68	3.27	4.57	3.24	2.99	4.50	4.50	2.42	2.42
P ₂ O ₅	0.09	0.12	0.07	0.05	0.06	0.10	0.14	0.16	0.13	0.11	0.11	0.09	0.22	0.24	0.27	0.26	0.20	0.10	0.32	0.40	0.83	0.83	0.18	0.18
PF	0.91	0.73	0.68	0.44	0.34	0.51	0.86	0.72	0.49	0.44	0.43	0.48	0.97	1.35	1.05	1.16	0.92	1.06	0.96	1.40	1.40	1.07	1.07	0.71
Total	99.37	98.96	99.81	99.64	99.81	98.24	100.44	98.99	100.29	100.44	100.51	99.36	100.85	100.84	100.41	99.93	100.13	99.28	100.38	100.89	100.23	100.23	100.04	100.04
V	21.91	42.00	12.30	6.20	10.60	21.09	35.28	55.05	9.78	23.98	26.92	30.68	68.17	162.80	60.94	88.60	34.91	40.75	118.40	90.29	214.70	51.47	51.47	51.47
Rb	128.3	174.0	229.0	194.1	169.0	156.7	135.6	174.7	146.8	198.2	232.3	120.9	148.5	199.6	199.6	137.0	179.2	118.7	314.3	188.8	463.5	205.0	205.0	205.0
Sr	216.9	291.0	121.0	107.8	125.0	191.9	313.1	257.6	200.2	187.3	190.1	307.0	315.3	255.6	329.5	467.0	201.1	388.1	167.9	342.5	195.6	106.2	106.2	106.2
Y	17.50	23.87	53.10	22.63	23.20	14.55	18.11	29.16	10.19	26.81	24.92	11.92	17.93	40.95	42.10	24.90	16.50	12.63	173.70	61.40	53.19	10.84	10.84	10.84
Zr	147	205	189	116	156	154	171	230	179	204	165	127	158	179	202	257	180	138	202	436	597	126	126	126
Nb	10.72	12.00	13.50	7.80	10.40	9.03	9.03	14.31	9.12	12.59	12.63	7.65	8.22	15.29	15.39	12.70	13.93	8.98	50.04	33.39	41.97	11.64	11.64	11.64
Ba	811	1257	342	382	363	786	837	827	858	649	544	776	377	301	571	1027	429	838	179	585	459	288	288	288
La	29.01	36.67	43.10	28.08	42.10	35.68	41.35	40.68	35.61	55.01	35.85	27.93	33.63	26.98	31.93	45.90	40.96	26.89	27.25	102.17	79.98	19.07	19.07	19.07
Ce	56.59	67.54	89.50	56.31	86.50	69.47	76.09	78.74	69.56	102.80	70.75	53.55	58.82	49.80	60.62	92.80	80.59	53.08	73.73	192.21	170.40	41.48	41.48	41.48
Pr	7.03	7.93	10.50	6.95	9.44	7.88	8.63	9.52	8.25	12.02	8.47	6.47	6.95	6.53	7.87	10.70	9.16	6.53	11.79	22.01	18.90	5.00	5.00	5.00
Nd	25.66	29.76	39.70	24.71	31.80	27.53	30.01	35.00	30.18	41.14	29.61	23.17	25.72	29.76	31.17	39.80	32.16	24.40	54.40	78.34	69.92	18.28	18.28	18.28
Sm	5.16	6.01	9.18	5.62	5.84	5.22	5.75	7.70	6.04	7.85	5.96	4.66	5.21	8.59	8.41	7.21	6.35	5.17	20.37	14.69	14.44	4.19	4.19	4.19
Eu	1.03	1.27	0.63	0.49	0.56	0.77	0.97	1.09	1.06	0.83	0.80	0.96	1.07	1.02	0.97	1.68	0.79	1.22	0.93	1.69	1.03	0.55	0.55	0.55
Gd	4.32	5.10	7.91	5.06	4.28	4.32	4.61	6.72	4.62	6.54	5.21	3.80	4.79	8.45	8.71	5.29	5.68	4.48	23.60	12.92	13.08	3.67	3.67	3.67
Dy	2.97	3.71	7.90	4.11	3.61	3.04	3.40	5.21	2.73	4.80	4.05	2.57	3.69	7.22	7.13	4.34	3.66	2.91	24.95	9.81	8.85	2.60	2.60	2.60
Ho	0.61	0.78	1.58	0.89	0.69	0.62	0.70	1.12	0.50	1.01	0.88	0.50	0.77	1.51	1.50	0.81	0.74	0.55	5.63	2.03	1.84	0.49	0.49	0.49
Er	1.68	2.23	4.72	2.44	1.99	1.60	1.90	3.01	1.28	2.64	2.47	1.29	1.90	3.94	3.86	2.18	1.77	1.34	16.22	6.09	4.77	1.20	1.20	1.20
Yb	1.57	2.09	5.09	2.49	2.14	1.54	1.87	2.93	1.05	2.69	2.94	1.27	1.73	3.57	3.68	2.18	1.40	1.18	18.53	6.33	4.11	1.18	1.18	1.18
Lu	0.21	0.32	0.77	0.35	0.33	0.22	0.27	0.43	0.15	0.39	0.44	0.18	0.25	0.51	0.52	0.33	0.19	0.16	2.81	0.89	0.57	0.18	0.18	0.18
Hf	4.44	5.47	6.56	4.09	5.28	4.58	5.10	6.74	5.82	6.17	5.32	3.81	4.31	4.78	6.70	6.49	5.29	3.87	8.36	11.96	15.44	4.21	4.21	4.21
Ta	0.79	0.88	2.04	0.77	1.20	0.65	0.88	1.42	0.70	0.98	1.75	0.64	0.48	0.73	2.17	1.15	0.64	0.59	9.68	3.02	1.76	2.22	2.22	2.22
W	6.48	0.79	14.60	1.79	2.19	5.99	7.80	4.44	1.12	2.38	1.69	0.26	2.57	1.05	<1	0.61	<1	18.08	5.99	2.98	1.34	<1	<1	<1
Pb	22.18	24.48	46.30	32.68	23.50	26.04	18.94	20.96	25.83	18.43	19.86	26.78	17.67	14.39	116.70	14.50	17.82	22.42	14.55	21.70	15.89	19.10	19.10	19.10
Th	12.43	12.85	33.40	24.27	24.70	12.92	17.62	14.05	14.48	21.68	19.91	10.43	8.06	3.80	13.41	12.90	11.60	7.93	9.10	39.06	19.38	9.52	9.52	9.52
U	2.42	3.44	12.00	7.02	4.97	1.78	3.12	3.66	3.62	4.38	6.50	4.21	2.55	2.93	4.74	4.03	2.70	2.25	4.63	17.09	2.75	1.47	1.47	1.47

Tin Bedjane		Monzogranite										Syenogranite										Enclaves		
Type	Syenogranite	Qz-monzodiorite					Granodiorite					Monzogranite					Syenogranite					Enclaves		
Sample	TOD55	TOD56	TOD46	J48	J47	J38	J35	J45	J45	J34	J36	J44	TOD51	TOD52	TOD70	TOD70	TOD71	J17	J43	TOD59	J16	TOD72	J36e	J36e
SiO ₂	76.10	75.90	57.34	64.83	64.92	66.62	65.60	65.94	66.43	69.14	74.80	68.66	65.36	65.07	65.07	65.43	69.51	76.05	74.77	74.07	52.25	60.99	60.99	60.99
TiO ₂	0.08	0.10	0.91	0.62	0.59	0.53	0.65	0.70	0.65	0.43	0.18	0.39	0.53	0.61	0.61	0.63	0.33	0.11	0.17	0.18	1.07	0.60	0.60	0.60
Al ₂ O ₃	12.72	12.70	17.06	15.43	15.41	15.72	15.33	15.51	15.31	14.59	12.96	15.04	15.80	15.07	15.07	15.48	14.94	12.61	12.91	13.57	13.24	14.46	14.46	14.46
Fe ₂ O ₃	0.03	0.01	1.11	1.82	1.72	4.76	4.13	4.52	5.00	4.82	3.86	4.67	5.25	5.08	5.08	4.92	3.19	1.61	2.16	2.21	12.83	7.47	7.47	7.47
MnO	0.03	0.01	0.11	0.08	0.07	0.06	0.07	0.07	0.07	0.06	0.03	0.07	0.08	0.07	0.08	0.06	0.04	0.03	0.04	0.03	0.18	0.14	0.14	0.14
MgO	0.05	0.10	2.65	2.18	2.04	1.47	0.97	1.23	1.34	1.25	0.28	0.41	0.71	1.63	1.63	1.73	0.56	0.07	0.20	0.28	7.37	3.		

Table 4 (Continued)

Type	Djanet Group									
	Detrital sedimentary rocks					Edembo rocks				
Sample	TOD40	TOD41	TOD44	TOD45	TOD47	Volcanic sills		Migmatite		Leucosome
						TOD43	TOD48	TOD67	TOD69	
Er	2.14	2.43	2.24	2.76	2.35	2.74	0.02	1.61	0.75	
Yb	2.21	2.55	2.26	2.84	2.35	2.73	0.00	1.66	0.78	
Lu	0.30	0.35	0.32	0.40	0.33	0.38	0.00	0.24	0.10	
Hf	3.86	4.99	4.12	4.58	4.59	4.17	2.59	5.25	3.33	
Ta	0.54	0.64	0.53	0.55	0.78	0.56	2.36	0.67	0.28	
W	33.74	6.04	7.29	5.55	27.08	6.02	48.60	0.03	11.98	
Pb	15.98	16.21	16.37	16.15	15.28	19.27	47.44	18.18	30.28	
Th	7.00	10.16	6.79	8.28	8.49	12.28	5.73	9.06	9.66	
U	1.55	1.90	1.57	2.58	1.73	4.01	5.40	1.51	1.21	

elements. Fe and Mn are close to NASC, Al, K and Ca are strongly depleted and Na is strongly enriched. Rb follows K and Sr, and to a lesser extent Ba, mirrors Na, reflecting the low abundance of K-feldspar and the high abundance of sodic plagioclase in the sediments of the Djanet Group.

Following the TAS (total alkali-silica) chemical classification (Le Maitre et al., 2002), the sill samples from the Djanet Group are trachyandesitic (TOD43) and rhyolitic (TOD48). The sample TOD43, with 58.6% SiO₂, is enriched in many elements including REE (Fig. 8C and D). Its Σ REE is 211 ppm, La_N = 117 and La_N/Yb_N = 10.6 with a moderately negative Eu anomaly (Eu/Eu* = 0.74; Fig. 8C). Rhyolite TOD48 has a REE pattern parallel to the trachyandesite from La to Sm but at much lower values (La_N = 14.4); it displays a strong Eu anomaly (Eu/Eu* = 0.18) and a spectacular decrease of HREE (Fig. 8C). The latter pattern is most probably linked to post-magmatic mobility during the greenschist-facies, which has been observed in Central Hoggar (Liégeois et al., 2003) and in the Anti-Atlas (Ennih and Liégeois, 2008). This agrees with the intense alteration seen in the thin section of this sample. The enrichment in REE for the trachyandesite is confirmed by the other trace elements (Fig. 8D). Considering the alteration effects, we interpret rhyolite sample TOD48 as a differentiated product of the trachyandesite.

4.2. The Djanet Batholith

Djanet Batholith granitoids contain 65–75% SiO₂, with enclaves that spread between 47% and 70% SiO₂. The Djanet Batholith exhibits a well-defined calc-alkalic trend on a MALI (Modified Alkali Lime Index) diagram (Fig. 9A; Frost et al., 2001) and a high-K calc-alkaline trend on a K₂O vs. SiO₂ diagram (Fig. 9B). These samples are metaluminous to slightly peraluminous, never crossing the 0.87 boundary in the SiO₂ vs. peralkaline index (Fig. 9C), above which are located most alkali-calcic and alkalic granitoids (Liégeois and Black, 1987). This is confirmed by plotting the analysis on a NYTS (normalized to Yenchichi–Telabit series) diagram (sliding normalization; Liégeois et al., 1998) based on trace elements. Samples from the Djanet Batholith all plot in the potassic domain (Fig. 9D) and are not related to an alkaline series.

The REE spectra from the Djanet Batholith (Fig. 10A) although superficially similar, have variable total REE (126 < Σ REE < 238 ppm) and REE fractionation (5 < La_N/Yb_N < 23), especially HREE fractionation (3 < La_N/Sm_N < 4.6, 0.9 < Dy_N/Lu_N < 1.8). The negative Eu anomalies are well marked (0.22 < Eu/Eu* < 0.68). The variation in HREE is greater than that of all other trace elements and is independent of silica (Fig. 10B). The felsic enclaves have similar spectra while mafic magmatic enclaves (MME) are enriched in LREE and especially in HREE (Fig. 10C). This suggests that the parent mafic magma of the Djanet Batholith was enriched in REE and that the variability in HREE in the granitoids is a result of magmatic differentiation. The abundance in large ion lithophile elements (LILE) can be correlated to silica, positively (K, Rb) or negatively (Sr, Ba) implying early crystallization of plagioclase and late crystallization of K-feldspar that did not separate from the magma, as seen in the field (Fig. 2D). Negative anomalies in P and Ti can be attributed to the fractionation of ilmenite, apatite and sphene. Apatite, due to its variable high abundance in REE (Hsieh et al., 2008) can induce variability in the REE abundance of the differentiating melt.

The biotite-rich enclaves and the xenolith corresponding to a rock from the Djanet Group have similar REE patterns to the Djanet Batholith granitoids (except for J8e with a flat REE pattern). This indicates that, although modified by different processes, these enclaves derive ultimately from calc-alkaline rocks and/or that they totally exchange trace elements with the enclosing granitoids. Sample J8e displays a seagull pattern typically resulting from a tetrad effect (enrichment in REE, especially HREE due to

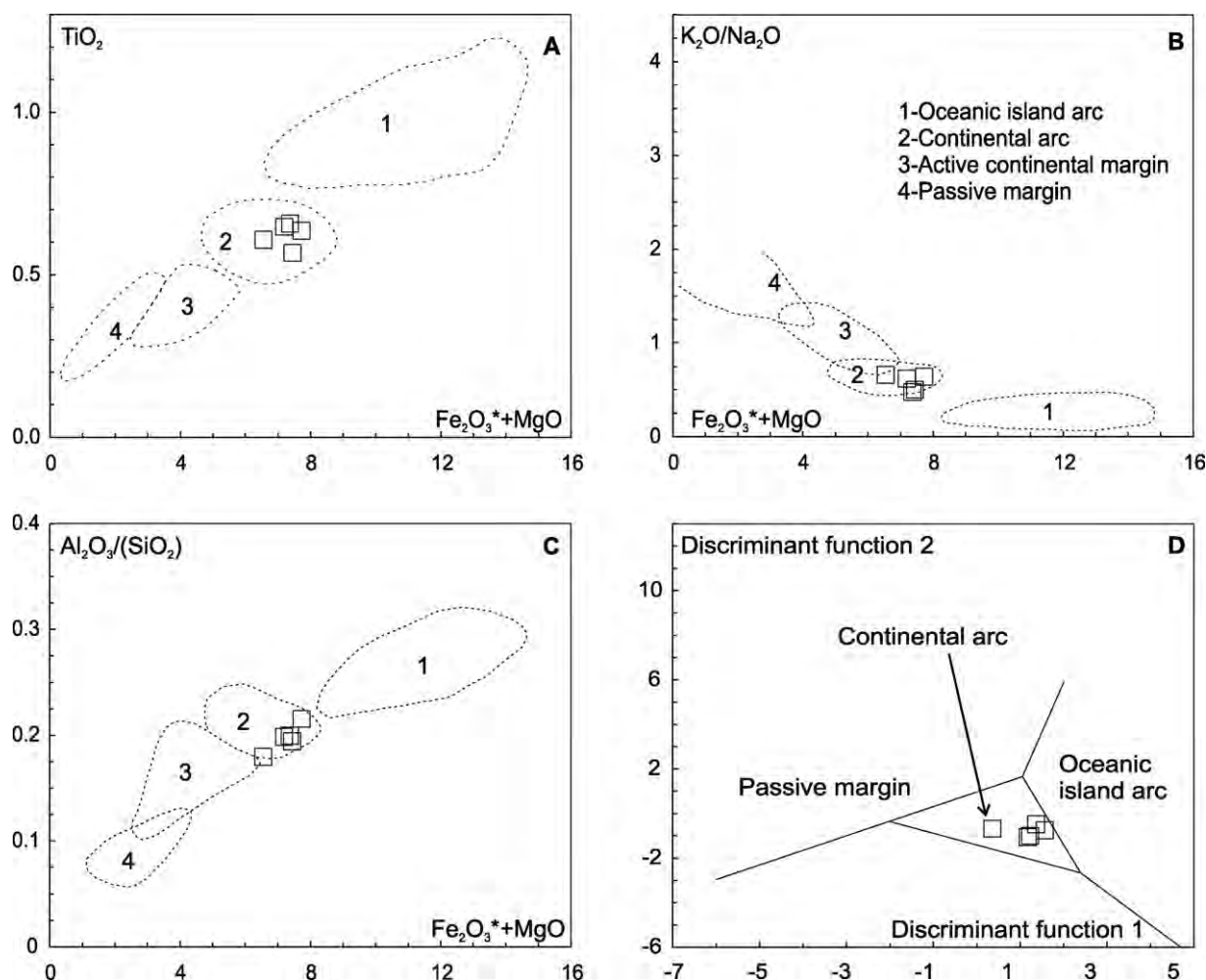


Fig. 7. Tectonic setting discrimination diagrams for the Djanet Group with discrimination fields after Bathia (1983) and Roser and Korsch (1986). Fe_2O_3^* represents total Fe expressed as Fe_2O_3 . (A) $\text{Fe}_2\text{O}_3^* + \text{MgO}$ vs. TiO_2 (Bathia, 1983), (B) $\text{Fe}_2\text{O}_3^* + \text{MgO}$ vs. $\text{K}_2\text{O}/\text{Na}_2\text{O}$ (Bathia, 1983), (C) $\text{Fe}_2\text{O}_3^* + \text{MgO}$ vs. $\text{Al}_2\text{O}_3/\text{SiO}_2$ (Bathia, 1983), (D) discriminant function diagram (Bathia, 1983); the discriminant functions are: function 1 = $(-0.0447 \times \text{SiO}_2) + (-0.972 \times \text{TiO}_2) + (0.008 \times \text{Al}_2\text{O}_3) + (-0.267 \times \text{Fe}_2\text{O}_3) + (0.208 \times \text{FeO}) + (-3.082 \times \text{MnO}) + (0.140 \times \text{MgO}) + (0.195 \times \text{CaO}) + (0.719 \times \text{Na}_2\text{O}) + (-0.032 \times \text{K}_2\text{O}) + (7.510 \times \text{P}_2\text{O}_5) + 0.303$; function 2 = $(-0.421 \times \text{SiO}_2) + (1.988 \times \text{TiO}_2) + (-0.526 \times \text{Al}_2\text{O}_3) + (-0.551 \times \text{Fe}_2\text{O}_3) + (-1.610 \times \text{FeO}) + (2.720 \times \text{MnO}) + (0.881 \times \text{MgO}) + (-0.907 \times \text{CaO}) + (-0.177 \times \text{Na}_2\text{O}) + (-1.840 \times \text{K}_2\text{O}) + (7.244 \times \text{P}_2\text{O}_5) + 43.57$.

F-rich fluids; Bau, 1996; Veksler et al., 2005). This process could also explain the variability in HREE observed in Djanet Batholith samples.

4.3. Tin Bedjane Pluton and Tin Amali Dyke Swarm

The Tin Bedjane Pluton is a syenogranite with some alkali-feldspar granites. The Tin Amali Dyke Swarm contains rocks mainly of granodioritic to monzogranitic/syenogranitic composition. These rocks belong to the calc-alkaline series including the syenogranites (Fig. 9A). They define a high-K to very high-K (“shoshonitic”) trend (Fig. 9B). They are metaluminous ($0.88 < \text{A}/\text{CNK} < 0.99$ for the dykes and $0.67 < \text{A}/\text{CNK} < 0.82$ for the enclaves) except the syenogranites that are slightly peraluminous ($1.01 < \text{A}/\text{CNK} < 1.02$). Their peralkaline index (PI; Fig. 9C) is comparable to that of the Djanet Batholith and varies between 0.54 and 0.84 except for the most fractionated sample J43 (PI=0.89). The sliding NYTS diagram based on trace elements confirms the potassic affinity of the Tin Bedjane Pluton and Tin Amali Dyke Swarm that do not belong to an alkaline series.

The two granites from the Tin Bedjane Pluton are strongly differentiated (76% SiO_2) and show evidence of feldspar fractionation: large negative Eu (Fig. 11A), Sr and Ba (Fig. 11B) anomalies. These

samples also show a strong apatite-ilmenite-sphene effect inducing strong negative P and Ti anomalies (Fig. 11B). This can be seen as an extreme case of the differentiation observed in the Djanet Batholith.

A similar process is observed in the Tin Amali Dyke Swarm. Granodioritic dykes (SiO_2 64–67%; Fig. 11C and D) have the lowest total REE ($170 < \Sigma\text{REE} < 184$ ppm), slight negative Eu anomalies ($0.85 < \text{Eu}/\text{Eu}^* < 0.91$), no Ba anomaly and only slight negative Ti and P anomalies. The most basic sample (TOD46: $\text{SiO}_2 = 47.3\%$), a quartz monzodiorite, has a more enriched REE spectrum with a slightly stronger negative Eu anomaly than the granodiorite dykes. In addition, it is characterized by low values of Ta, Hf, Zr and enrichment in P, Ti, Y, Yb. These differences are possibly related to its primitive composition. Monzogranitic dykes (SiO_2 65–70%; Fig. 11E and F) are richer in REE ($212 < \Sigma\text{REE} < 298$ ppm), have larger Eu negative anomalies ($0.51 < \text{Eu}/\text{Eu}^* < 0.84$) and stronger Ti–P anomalies, but have no Ba anomaly. The less pronounced anomalies, at similar silica content compared to granitoids from the Djanet batholith can be attributed to faster ascent in the crust, leaving less time for crystals to settle and hence to produce negative anomalies. Negative anomalies occur only in the most differentiated syenogranite and monzogranite samples (J44: $\text{SiO}_2 = 74.8\%$), maybe through filter pressing. These samples (SiO_2 74–76%; Fig. 11G and H) are

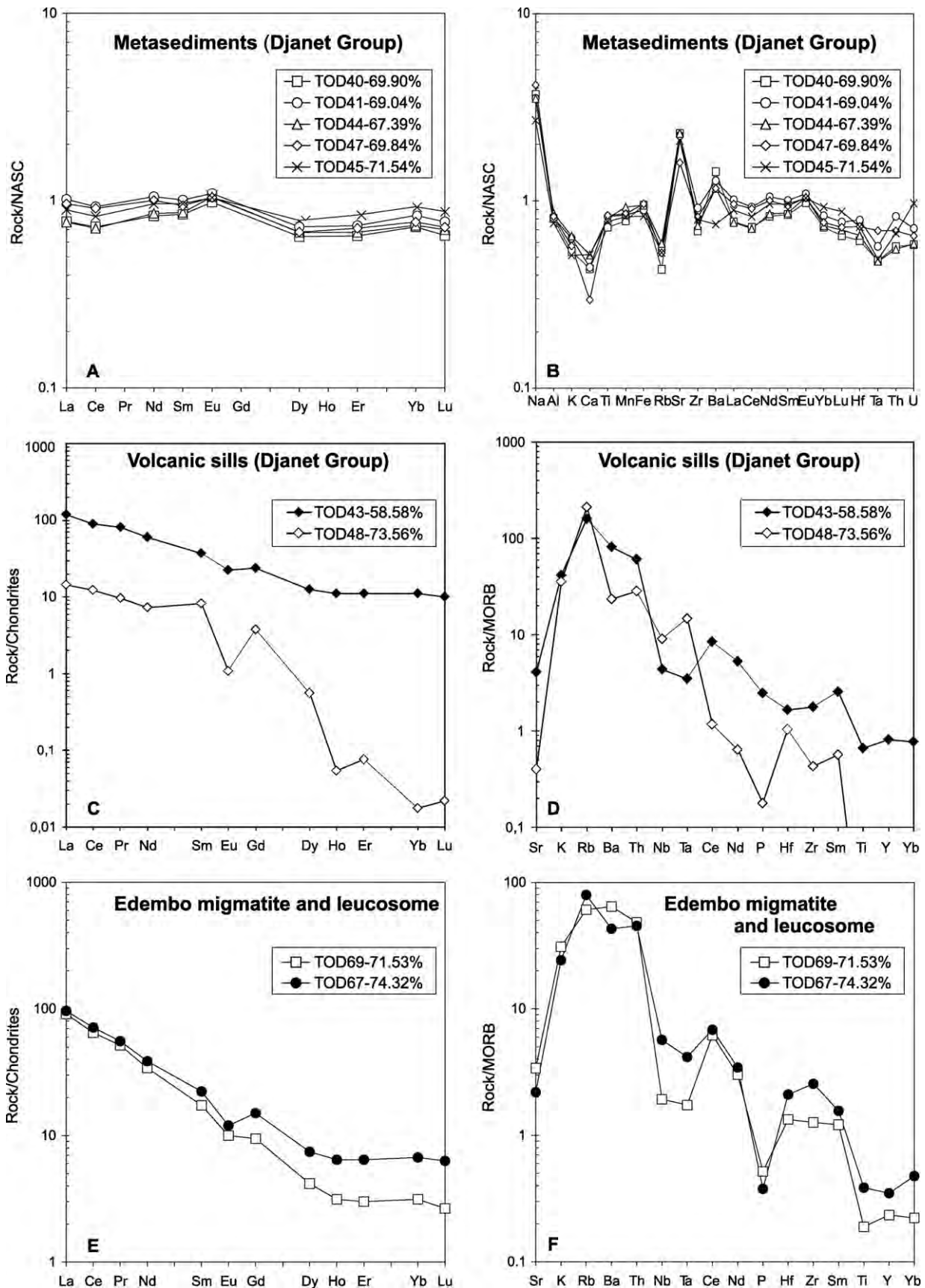


Fig. 8. Geochemistry of the Djanet Group, metasediments (A and B) and associated volcanic sills (C and D) and of the Edembo migmatitic Ouhot Group (E and F): (A) REE of the Djanet metasediments normalized to NASC (North American Schist Composite; Gromet et al., 1984); (B) trace elements of the Djanet metasediments normalized to NASC; (C) REE of the Djanet sills normalized to chondrite (Taylor and Mc Lennan, 1985); (D) trace elements of the Djanet sills normalized to MORB (Sun, 1980; Pearce, 1982). (E) REE diagram normalized to chondrite (Taylor and Mc Lennan, 1985) for the Edembo migmatite and leucosome; (F) trace elements normalized to MORB (Sun, 1980; Pearce, 1982) for the Edembo migmatite and leucosome. Value next to the sample number is the silica content.

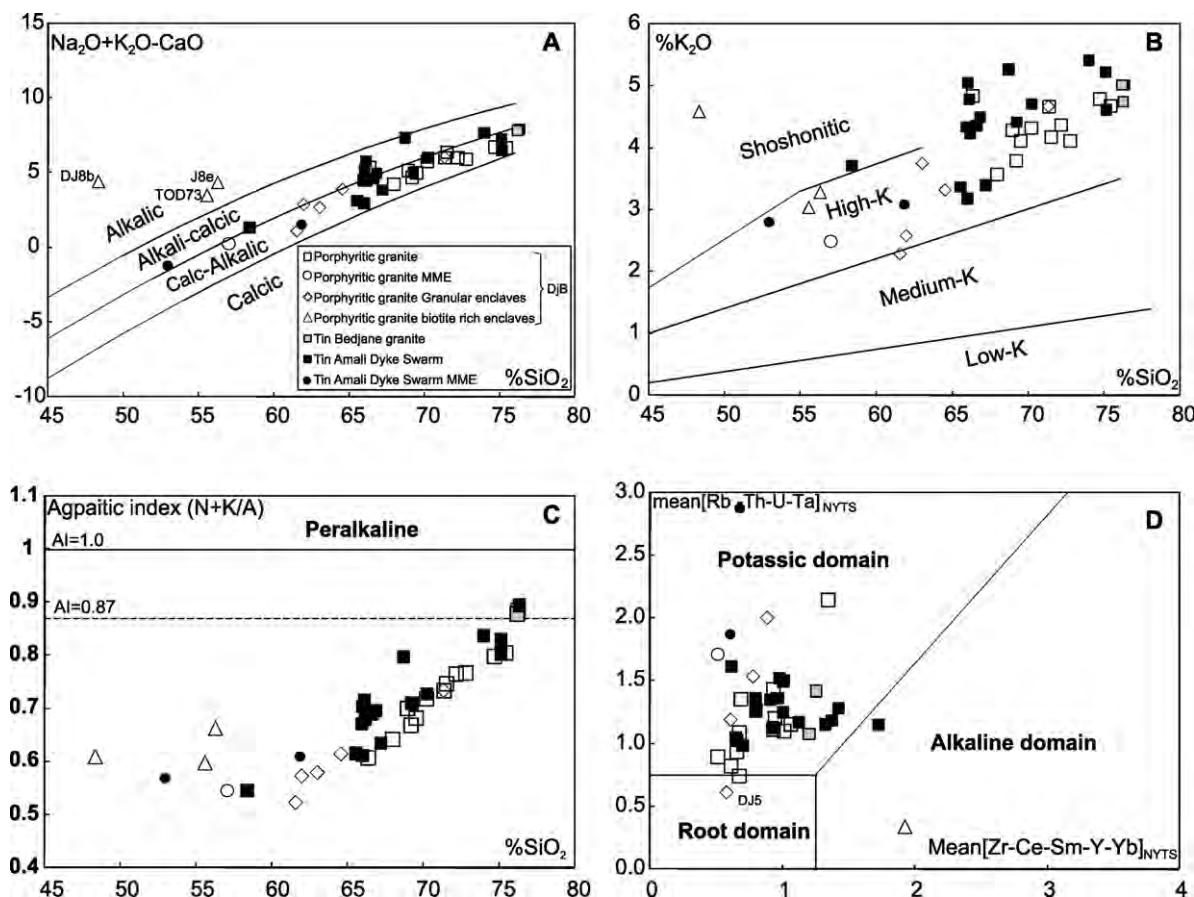


Fig. 9. Major element diagrams for the Djanet Batholith, Tin Bedjane Pluton and Tin Amali Dyke Swarm: (A) $\text{Na}_2\text{O} + \text{K}_2\text{O} - \text{CaO}$ vs. SiO_2 (MALL, Frost et al., 2001); (B) SiO_2 vs. K_2O (subdivisions from Rickwood, 1989); (C) SiO_2 vs. peralkaline index ($[(\text{K}_2\text{O} + \text{Na}_2\text{O})/\text{Al}_2\text{O}_3]$ in molar proportions); $\text{Al} = 0.87$ from Liégeois and Black (1987) separating the calc-alkaline series from the metaluminous alkaline series; (D) sliding normalized values to the Yenchichi-Telabit reference series (Liégeois et al., 1998).

even richer in REE ($279 < \Sigma\text{REE} < 302$ ppm) but have strong negative anomalies in Eu ($0.16 < \text{Eu}/\text{Eu}^* < 0.26$) Ba, Ti and P, although less marked than in samples of similar silica content of the Tin Bedjane Pluton ($0.05 < \text{Eu}/\text{Eu}^* < 0.12$, $148 < \Sigma\text{REE} < 185$).

The difference in geochemistry between the Djanet Batholith, the Tin Bedjane Pluton and the Tin Amali Dyke Swarm can then be ascribed to differentiation and to the conditions in which this differentiation occurred, such that the same source can be postulated for them. This interpretation is in agreement with the similar ages of these magmatic bodies.

4.4. The Edembo migmatites and associated granite

The two migmatite and associated granite samples have granodioritic composition and are peraluminous. The REE and trace element spectra of the migmatite TOD67 are similar to those of the Djanet Group spectra (Fig. 8E and F), differing only in their lower HREE abundances, slight positive Zr anomaly and negative Y anomaly. The Djanet Group (Fig. 8C and D) could be protolith for the Ouhot migmatites (Fig. 8E and F), a hypothesis that is sustained by the similar age of their respective detrital zircon populations.

The two-mica granitic leucosome TOD69 is impoverished in ΣREE , but especially in HREE. This could be related to the abundance of HREE-enriched garnet in the migmatites, giving a status of migmatitic differentiated melt to this granite, the garnet being absent in the leucosome. This agrees with the low abundance of most of the trace elements in the granitic leucosome when compared to the migmatite (Fig. 8E and F).

5. Sr and Nd isotopes

Sr and Nd isotopes have been measured on 45 samples: 7 samples from the Djanet Group (5 sediments and 2 sills), 1 sample from the Edembo migmatitic Ouhot Complex, 22 samples from the Djanet Batholith (12 granitoids and 10 enclaves), 2 samples from the Tin Bedjane Pluton and 13 samples from the Tin Amali Dyke Swarm (12 dykes and 1 enclave). Results are given in Tables 5 and 6 and analytical techniques in the appendix.

5.1. Results

The initial $^{87}\text{Sr}/^{86}\text{Sr}$ (Sr_i) of the Djanet Batholith at 571 Ma varies from 0.7052 to 0.7095. The initial $^{143}\text{Nd}/^{144}\text{Nd}$ relative to CHUR at 571 Ma (ε_{Nd}) also vary significantly, from -3 to -11 , leading to a trend pointing to an old Rb-depleted continental source (Fig. 12). The enclaves, mafic to felsic, have similar Nd isotopic signatures (ε_{Nd} from -3.8 to -9) but sometimes lower Sr_i . Biotite amphibole enclaves vary from 0.7016 to 0.7062, the mica-rich enclave from 0.7032 to 0.7073 and the Djanet Group xenolith has a low Sr_i of 0.7005, most likely not primary.

The Sr_i in the Tin Amali Dyke Swarm vary from 0.6426 to 0.7092. This indicates that these isotopic ratios have been disturbed after their emplacement. Indeed, these samples define an errorchron (MSWD = 5.2 for 10 samples) giving a Devonian age of 387 ± 17 Ma ($\text{Sr}_i = 0.70739 \pm 0.00069$). Doleritic dykes and sills in southern Hoggar are c. 350 Ma (Djellit et al., 2006) while the Air ring-complexes in Niger are c. 410 Ma (Moreau et al., 1994). By analogy, this suggests that tectonic movements accompanied by fluid percolation

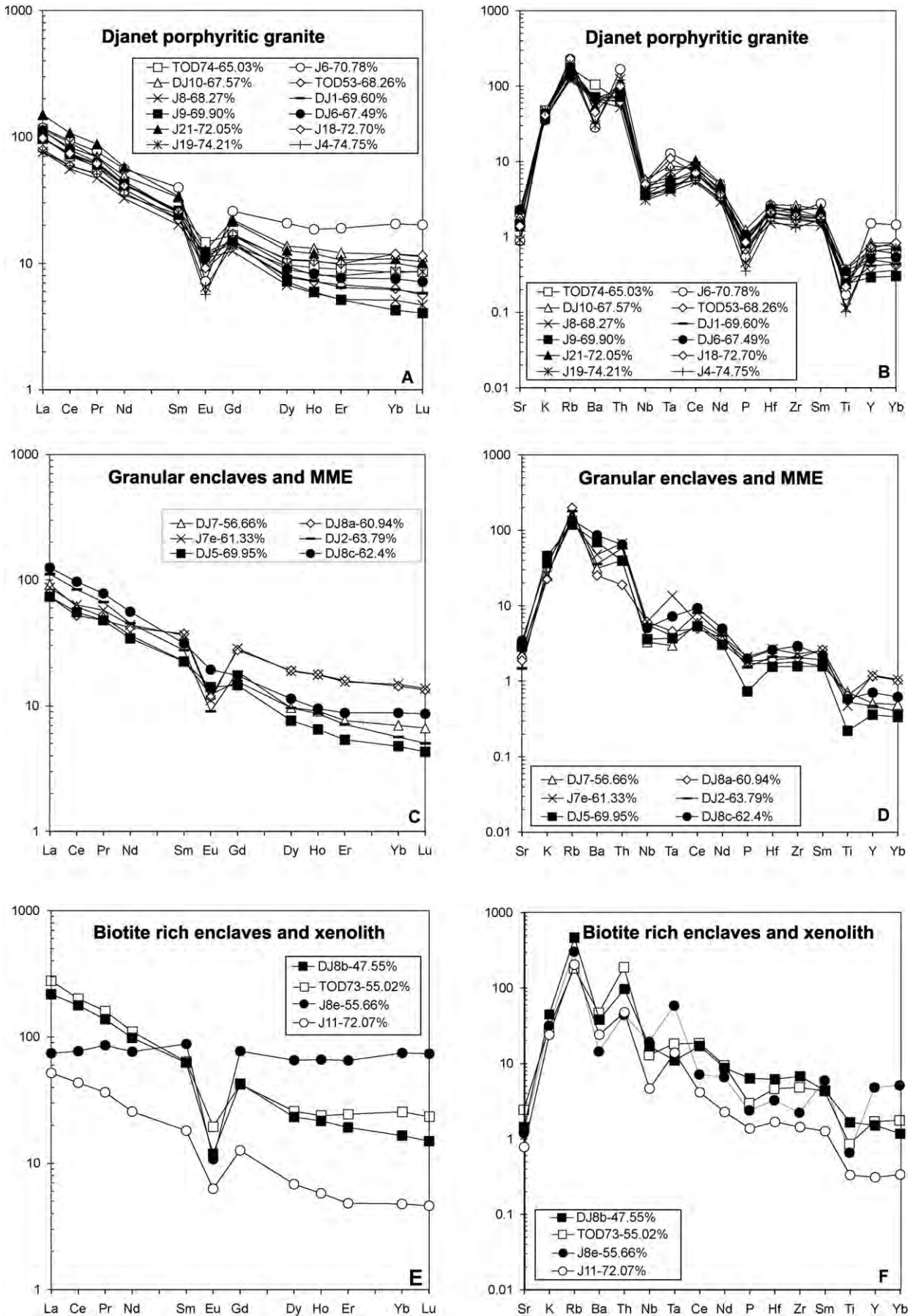


Fig. 10. Trace elements diagrams for the granitoids and associated enclaves of the Djanet Batholith. A, C and E are normalized to chondrite (Taylor and Mc Lennan, 1985) and B, D and F are normalized to MORB (Sun, 1980; Pearce, 1982); value next to the sample number is the silica content.

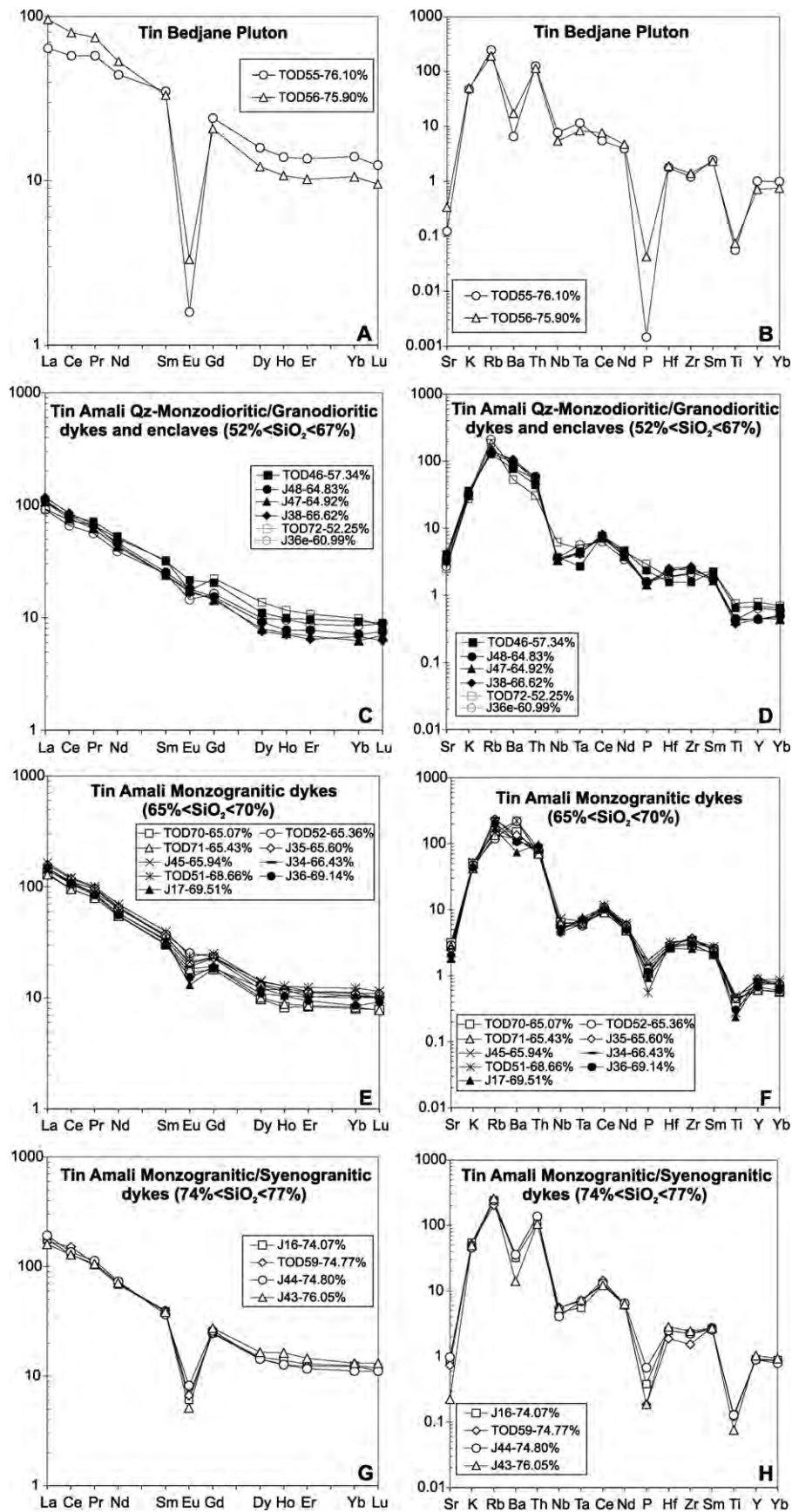


Fig. 11. REE normalized to chondrite (Taylor and Mc Lennan, 1985) and trace elements normalized to MORB (Sun, 1980; Pearce, 1982) diagrams, respectively, for the Tin Bedjane Pluton (A and B) and the Tin Amali Dyke Swarm (C–H).

Table 5
Rb–Sr and Sm–Nd isotopes on whole rock for the Djanet Group and Edembo migmatite.

Sample	Rb	Sr	$^{87}\text{Rt}/^{86}\text{Sr}$	$^{87}\text{Rt}/^{86}\text{Sr}$	$^{87}\text{Rt}/^{86}\text{Sr}$	2σ	Sr_i 600Ma	Sr_i 571Ma	Sm	Nd	$^{147}\text{Sm}/^{144}\text{Nd}$	$^{143}\text{Nd}/^{144}\text{Nd}$	2σ	ϵ_{Nd} 600Ma	ϵ_{Nd} 571Ma	T_{DM}
Djanet group																
Sediments																
TOD40	54	326	0.4783	0.711021	0.000011	0.000011	0.706929	0.707127	4.72	22.65	0.1260	0.512386	0.000006	0.50	0.24	1143
TOD41	68	318	0.6240	0.711559	0.000009	0.000009	0.706220	0.706479	5.62	28.79	0.1181	0.512205	0.000010	-2.43	-2.72	1334
TOD44	74	326	0.6588	0.712256	0.000009	0.000009	0.706619	0.706893	4.82	23.37	0.1247	0.512239	0.000006	-2.27	-2.53	1374
TOD45	66	298	0.6439	0.710677	0.000013	0.000013	0.705167	0.705435	5.39	26.36	0.1236	0.512340	0.000006	-0.21	-0.48	1189
TOD47	66	227	0.8402	0.715308	0.000010	0.000010	0.708119	0.708468	5.25	27.47	0.1156	0.512140	0.000007	-3.50	-3.80	1400
Dykes																
TOD43	162	559	0.8385	0.713934	0.000010	0.000010	0.706759	0.707107	8.53	42.36	0.1218	0.512030	0.000012	-6.12	-6.40	1675
TOD48	213	54	11.4436	0.811858	0.000012	0.000012	0.713942	0.718694	1.88	5.17	0.2205	0.512554	0.000009	-3.47	-3.38	-
Edembo migmatite																
TOD67	80	298	0.7744	0.715645	0.000010	0.000010	0.709019	0.709340	5.16	27.51	0.1134	0.511977	0.000007	-6.52	-6.83	1616

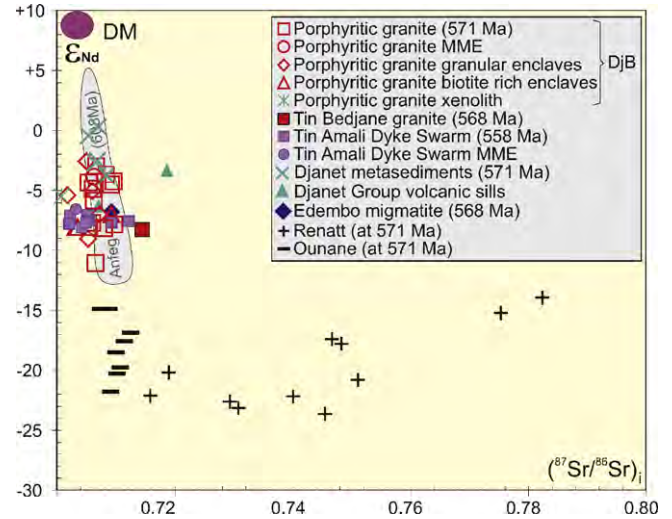


Fig. 12. Sr and Nd isotopic initial ratios (ϵ_{Nd} vs. $(^{87}\text{Sr}/^{86}\text{Sr})_i$) for the studied rocks and for some references from the Tuareg Shield (Anfeg batholith from *Acef et al., 2003*, Renatt granite from *Liégeois et al., 1994*, Ounane granitoids from *Liégeois et al., 2003*). DjB = Djanet Batholith.

probably occurred at this period along the Tin Amali shear zone – a boundary terrane – along which the Tin Amali Dyke Swarm intruded at 558 ± 6 Ma. The magmatic Sr_i at 558 Ma for the Tin Amali Dyke Swarm cannot thus be calculated with precision but was lower than 0.7074, the mean initial ratio at 387 Ma.

In contrast, the Nd isotopic compositions of Tin Amali Dyke Swarm have not been affected by Devonian events due to the relative immobility of the REE. The ϵ_{Nd} values at 558 Ma group between -6.5 and -8.1 and show less variation compared to the Djanet Batholith.

The two samples from the Tin Bedjane Pluton have high to very high Sr_i at 568 Ma (0.7144–0.7439), which may have resulted from the Devonian reactivation of the shear zone. The similar ϵ_{Nd} at $c. -8.5$ of the pluton supports that model.

Single-stage Nd T_{DM} model ages assume that there was no change of Sm/Nd during the magma generation, the magma having similar ratio as its source. This assumption is reasonable for the studied rocks except for those affected by the REE tetrad effect. Unaffected samples have $^{147}\text{Sm}/^{144}\text{Nd}$ between 0.11 and 0.13, which correspond to the mean of the continental crust. For rocks affected by late magmatic events (which, by opposition to the Devonian event are not detected by isotopic ratios, no measurable decay having yet occurred), there is the need to use the mean continental $^{147}\text{Sm}/^{144}\text{Nd}$ of 0.12 for the period before intrusion (two-stage Nd T_{DM} model ages; *Table 6*; see *Liégeois and Stern, 2010* for additional discussion on T_{DM} model ages). In unaffected rocks, single-stage and two-stage model ages are very similar. Two-stage model ages for the Djanet Batholith (granitoids and enclaves) vary between 1338 and 2048 Ma, with a mean of 1637 ± 82 Ma. The Tin Bedjane Pluton falls within the range of the Djanet Batholith (1742–1820 Ma, mean = 1780 ± 55 Ma). Two-stage model ages for the Tin Amali Dyke Swarm vary between 1660 and 1787 Ma, with a mean of 1730 ± 17 Ma. The three means agree within 100 m.y. and support the contention that the different igneous suites from the Djanet Terrane originated from the same source.

The metasediments from the Djanet Group have Sr_i varying from 0.7051 to 0.7081 at 600 Ma and from 0.7054 to 0.7085 at 570 Ma. The ϵ_{Nd} values vary between $+0.5$ and -3.5 at 600 Ma and between $+0.2$ and -3.8 at 570 Ma. These values are more depleted than those of the Djanet intrusives or close to the more depleted samples of these granitoids. Their Nd T_{DM} model ages are between 1140 and 1400 Ma. Dykes from the Djanet Group and the Edembo migmatite

Table 6
Sm–Nd isotopes and Rb–Sr isotopes on whole rock for the Djanet Batholith, Tin Bedjane Pluton and Tin Amali Dyke Swarm.

Sample	Rb	Sr	⁸⁷ Rb/ ⁸⁶ Sr	⁸⁷ Sr/ ⁸⁶ Sr	2σ	Sr _i	Sm	Nd	¹⁴⁷ Sm/ ¹⁴⁴ Nd	¹⁴³ Nd/ ¹⁴⁴ Nd	2σ	ε _{Nd} (571 Ma)	TDM1 1 stage	TDM2 2 stage
Djanet batholith														
Monzogranite TOD53	128	217	1.714	0.722177	0.000010	0.708218	5.16	25.66	0.1216	0.512170	0.000009	-3.65	1441	1429
Monzogranite TOD74	168	317	1.535	0.720374	0.000010	0.707873	5.83	30.05	0.1174	0.511925	0.000005	-8.13	1766	1802
Monzogranite J4	194	108	5.233	0.751740	0.000015	0.709137	5.62	24.71	0.1376	0.512185	0.000012	-4.53	1712	1501
Monzogranite J6	229	121	5.501	0.754308	0.000008	0.709516	9.18	39.70	0.1398	0.512207	0.000012	-4.26	1719	1479
Monzogranite J19	169	125	3.925	0.741630	0.000010	0.709672	5.84	31.80	0.1111	0.511916	0.000019	-7.30	1670	1778
Monzogranite DJ1	157	192	2.367	0.725451	0.000007	0.706180	5.22	27.53	0.1146	0.512031	0.000009	-5.86	1552	1612
Monzogranite DJ6	136	313	1.254	0.716298	0.000010	0.706086	5.75	30.01	0.1159	0.512087	0.000008	-4.86	1486	1529
Monzogranite DJ10	175	258	1.965	0.722498	0.000009	0.706497	7.70	35.00	0.1330	0.511834	0.000010	-11.05	2288	2048
Monzogranite J9	147	200	2.125	0.723912	0.000012	0.706609	6.04	30.18	0.1209	0.512203	0.000009	-2.96	1377	1372
Monzogranite J21	198	187	3.069	0.730976	0.000012	0.705989	7.85	41.14	0.1154	0.511940	0.000009	-7.70	1707	1765
Monzogranite J18	232	190	3.545	0.734285	0.000009	0.705421	5.96	29.61	0.1217	0.511944	0.000009	-8.07	1816	1797
Granodiorite J8	121	307	1.140	0.714614	0.000010	0.705330	4.66	23.17	0.1215	0.512134	0.000008	-4.35	1499	1487
MME DJ7	149	315	1.364	0.717326	0.000009	0.706220	5.21	25.72	0.1226	0.512163	0.000011	-3.86	1468	1446
Granular enclave DJ8a	200	256	2.263	0.723690	0.000010	0.705264	8.59	29.76	0.1745	0.512092	0.000008	-9.04	3946	1878
Granular enclave J7e	134	330	1.173	0.715472	0.000010	0.705920	8.41	31.17	0.1631	0.512255	0.000008	-5.03	2385	1543
Granular enclave DJ2	179	201	2.582	0.722754	0.000010	0.701730	6.35	32.16	0.1194	0.512073	0.000013	-5.39	1564	1573
Granular enclave DJ5	119	388	0.885	0.712200	0.000010	0.704991	5.17	24.40	0.1281	0.512251	0.000008	-2.55	1407	1338
Granular enclave DJ8c	137	467	0.849	0.714083	0.000009	0.707167	7.21	39.80	0.1096	0.511953	0.000012	-7.01	1592	1708
Biotite-rich enclave J8e	314	168	5.438	0.747357	0.000010	0.703083	20.37	54.40	0.2265	0.512337	0.000009	-8.06	9015	1795
Biotite-rich enclave TOD73	189	342	1.597	0.722173	0.000012	0.709167	14.69	78.34	0.1134	0.511968	0.000010	-7.00	1629	1707
Biotite-rich enclave DJ8b	464	196	6.892	0.759517	0.000012	0.703406	14.44	69.92	0.1249	0.511958	0.000014	-8.04	1859	1794
Xenolith J11	205	106	5.607	0.746400	0.000007	0.700750	4.19	18.28	0.1385	0.512139	0.000010	-5.50	1828	1582
Tin Bedjane pluton														
Syenogranite TOD55	248	17	44.209	1.101997	0.000013	0.743987	8.10	31.48	0.1556	0.512043	0.000009	-8.64	2650	1742
Syenogranite TOD56	192	46	12.281	0.813923	0.000010	0.714462	7.66	37.92	0.1222	0.511932	0.000009	-8.38	1847	1820
Tin Amali dyke swarm														
Granodiorite J48	133	448	0.857	0.711866	0.000009	0.704949	5.87	32.99	0.1075	0.511951	0.000008	-6.96	1564	1701
Granodiorite J47	147	571	0.743	0.711601	0.000007	0.705598	5.52	30.46	0.1096	0.511935	0.000010	-7.42	1618	1739
Granodiorite J38	142	500	0.819	0.711751	0.000007	0.705138	5.58	31.70	0.1064	0.511923	0.000011	-7.43	1588	1740
Monzogranite J35	235	341	1.994	0.718016	0.000011	0.701923	8.28	47.00	0.1065	0.511930	0.000007	-7.39	1579	1729
Monzogranite J45	171	312	1.582	0.716677	0.000011	0.703909	8.27	45.33	0.1103	0.511936	0.000011	-7.54	1628	1741
Monzogranite J34	247	346	2.067	0.718344	0.000007	0.701657	7.74	41.00	0.1142	0.511937	0.000013	-7.72	1691	1763
Monzogranite J36	208	273	2.205	0.719521	0.000009	0.701725	6.98	39.26	0.1075	0.511938	0.000008	-7.30	1582	1721
Monzogranite J44	241	134	5.219	0.738047	0.000007	0.695930	8.45	52.07	0.0982	0.511927	0.000010	-6.75	1470	1684
Monzogranite J17	170	243	2.028	0.725298	0.000007	0.709165	7.59	41.10	0.1117	0.511932	0.000012	-7.72	1656	1756
Syenogranite J43	259	30	25.221	0.843225	0.000007	0.639697	8.94	50.72	0.1066	0.511943	0.000010	-7.05	1562	1708
Syenogranite TOD59	205	100	5.929	0.759495	0.000008	0.711651	9.14	49.73	0.1112	0.511934	0.000006	-7.64	1645	1750
Syenogranite J16	242	123	5.705	0.750109	0.000011	0.704719	8.96	48.65	0.1114	0.511931	0.000012	-7.72	1653	1756
MME J36c	210	374	1.624	0.715999	0.000007	0.702888	5.69	27.77	0.1240	0.512036	0.000011	-6.49	1706	1660

have Sr and Nd isotope signatures, including Nd T_{DM} model ages, similar to the Djanet intrusives.

5.2. Origin of Djanet Terrane rocks

The c. 1.7 Ga Nd model age indicates that old continental crust (2 Ga old or older, maybe Archaean, with some influence from a juvenile Neoproterozoic source) was melted to generate Djanet igneous rocks. This can be shown in a diagram of Sr_1 vs. ϵ_{Nd} (Fig. 12) where data from the Tuareg terranes to the west have been added (for their localities see Fig. 1A); the Anfeq batholith, resembling the Djanet Batholith and intruded at 608 ± 7 Ma (Bertrand et al., 1986, recalculated by Acef et al., 2003) the LATEA metacraton, the Ounane batholith in NE LATEA (624 ± 15 Ma; Liégeois et al., 2003) and the Renatt granite (c. 600 Ma, Liégeois et al., unpublished results) in the Assodé-Issalane terrane in Air (Niger) for which Sr and Nd isotopic ratios are available (Acef et al., 2003; Liégeois et al., 2003; Liégeois et al., 1998, respectively). The Renatt granite is a typical crustal migmatitic-associated leucogranite and gives two old continental crustal signatures, one Rb-depleted and the other not; the Ounane batholith converges to the Rb-depleted old crustal signature. The Anfeq batholith, representative of most of the Tuareg Pan-African batholith (for other batholith references, see Liégeois et al., 1998), lies in between the Rb-depleted crust and the depleted mantle, which has been interpreted as the result of the mixing in various proportions between juvenile mantle magma heating the old crust and the magma resulting from the melting of the latter (Acef et al., 2003; Liégeois et al., 1998, 2003). This model can also be applied to the magmatic suite of the Djanet Terrane, from the Djanet Batholith to the Tin Amali Dyke Swarm.

It can be concluded that the three magmatic phases in the Djanet Terrane (Djanet Batholith, Tin Bedjane Pluton, Tin Amali Dyke Swarm) originated from an old continental crustal source (Palaeoproterozoic in age, likely to be associated with some Archaean rocks) that melted during intrusion of mantle-derived magmas (see below the model). The mantle and crustal magmas mixed in variable proportions but with a predominance of the old crustal component.

The metasediments have Sr and Nd isotopic initial ratios more depleted than most Djanet intrusive rocks and are in the range of the Anfeq batholith from the LATEA metacraton (Fig. 1A), in agreement with a source mainly in Central Hoggar. The fact that they are located in the more depleted part of the Anfeq field could be a consequence of the presence of a more juvenile component in their source as suggested by the geochemistry, which can be present for example in Serouenout or Aouzegueur Terranes (Fig. 1A). This is also reflected by their younger Nd T_{DM} model ages between 1140 and 1400 Ma.

6. Metacratonic evolution of the Djanet Terrane

Contrasting behaviour has been observed for the Djanet and Edembo Terranes during the upper Ediacaran. Djanet Group sediments were deposited a short time after 590 Ma (youngest detrital zircon) and was deformed and metamorphosed before and at 570 Ma (intrusion of Djanet Batholith and Tin Bedjane Pluton). They have only been affected by greenschist-facies metamorphism in the Djanet Terrane at c. 570 Ma but were migmatized in the Edembo Terrane at the same time (568 ± 4 Ma). The two types of metamorphic rocks can be located very close, on both sides of the shear zone separating the two terranes.

No older Neoproterozoic events have been recorded such as the main Pan-African batholithic stage present in the LATEA metacraton (630–580 Ma; Acef et al., 2003; Liégeois et al., 2003; Abdallah et al., 2007) and no one rock with an oceanic affinity has been mapped

or seen. The oldest event is the deposition of the Djanet Group that occurred between 590 and 570 Ma (i.e. 580 ± 10 Ma). Detrital zircon ages recorded in these sediments (from 630 Ma to Archaean, without Mesoproterozoic ages) correspond to the various ages known to the west in Central Hoggar (LATEA metacraton) whose Pan-African evolution stopped with the emplacement of high-level plutons at c. 580 Ma (Abdallah et al., 2007). The deposition of the Djanet Group occurred then during the final uplift of the LATEA metacraton on the non-uplifted area that was the Eastern Hoggar. Eastern Hoggar can be considered as a relatively stable area during the deposition of the Djanet Group (580 ± 10 Ma).

By opposition, the Djanet Group was affected by a transpressive event accompanied by magmatism and metamorphism in the Edembo and Djanet terranes. The more westerly lying Aouzegueur Terrane has also been intruded by c. 555 Ma old granites and greenschist-facies metamorphism but following a more complex evolution (Henry et al., 2009). This event is not known to the west of the Raghane shear zone, in Central and Western Hoggar except maybe through ring-complexes (Taourirt Province; Azzouini-Sekkal et al., 2003) or through brittle faults and quartz dykes (Liégeois et al., 1994). The transpressive character of the deformation and the non-alkaline nature of the magmatism exclude a rift environment. Regional subhorizontal stretching mineral lineation implies some horizontal relative movement between Edembo and Djanet terranes. However, the similar pre-deformation sedimentary sequence with a same Central Hoggar source, absence of oceanic rocks and the likely short life of this event (575–555 Ma) are not in favour of a large relative movement and not in favour of considering these two terranes as completely allochthonous.

Another explanation must be found for explaining the contrasted behaviour of the Edembo and Djanet Terranes during the late Ediacaran. We propose here that this is due to the presence of a craton to the east, below the Murzuk basin (Fig. 13). Looking at the recent geophysical data about crustal and lithospheric thickness of Africa (Pasyanos and Nyblade, 2007), it is noteworthy that the Murzuq basin is underlain by 40 km thick crust and by 250 km thick lithosphere, which is much more than that underlying the neighbouring areas (Fig. 14), supporting a truly cratonic status. The existence of a Murzuq Craton is sustained by additional observations: (1) the subcircular shape of the Murzuq basin and its long-lasting sedimentation (Ordovician to Carboniferous but also Mesozoic and Cenozoic; Fig. 13) is typical of cratonic areas (Black and Liégeois, 1993); (2) the characteristically young Pan-African ages of the magmatic suites of the Djanet Terrane intruded in greenschist-facies sediments, has also been described in western Tibesti (El Makhrouf, 1998; Suayah et al., 2006), suggesting that the Western Tibesti (“Upper Tibestian”) could be the south-eastern equivalent to the Djanet Terrane. Let us remark that if magmatism in the range 570–550 Ma is known elsewhere in Northern Africa, it always corresponds to late minor events preceded by a climax episode at around 600 Ma (e.g. Liégeois and Black, 1987; Moussa et al., 2008), which is not the case here.

In that configuration, the Djanet Terrane would correspond to the reactivated boundary of the Murzuk craton, the thick lithosphere of the latter preventing more important effects than fracturation of the lithosphere allowing magmas to rise and greenschist-facies metamorphism. This corresponds to a metacratonic evolution (Abdelsalam et al., 2002; Liégeois et al., 2003; De Waele et al., 2006; Ennih and Liégeois, 2008), the Djanet Terrane (and possibly Western Tibesti) being the metacratonic margin of the Murzuk craton. In contrast, the Edembo Terrane was much more affected and behaved as a mobile belt, in agreement with a thinner lithospheric mantle. As the magmatism present in the Djanet Terrane is always close to the shear zone delimiting the two terranes, it is probable that its melting source is actually located below the Edembo Terrane rather than below the Djanet Terrane

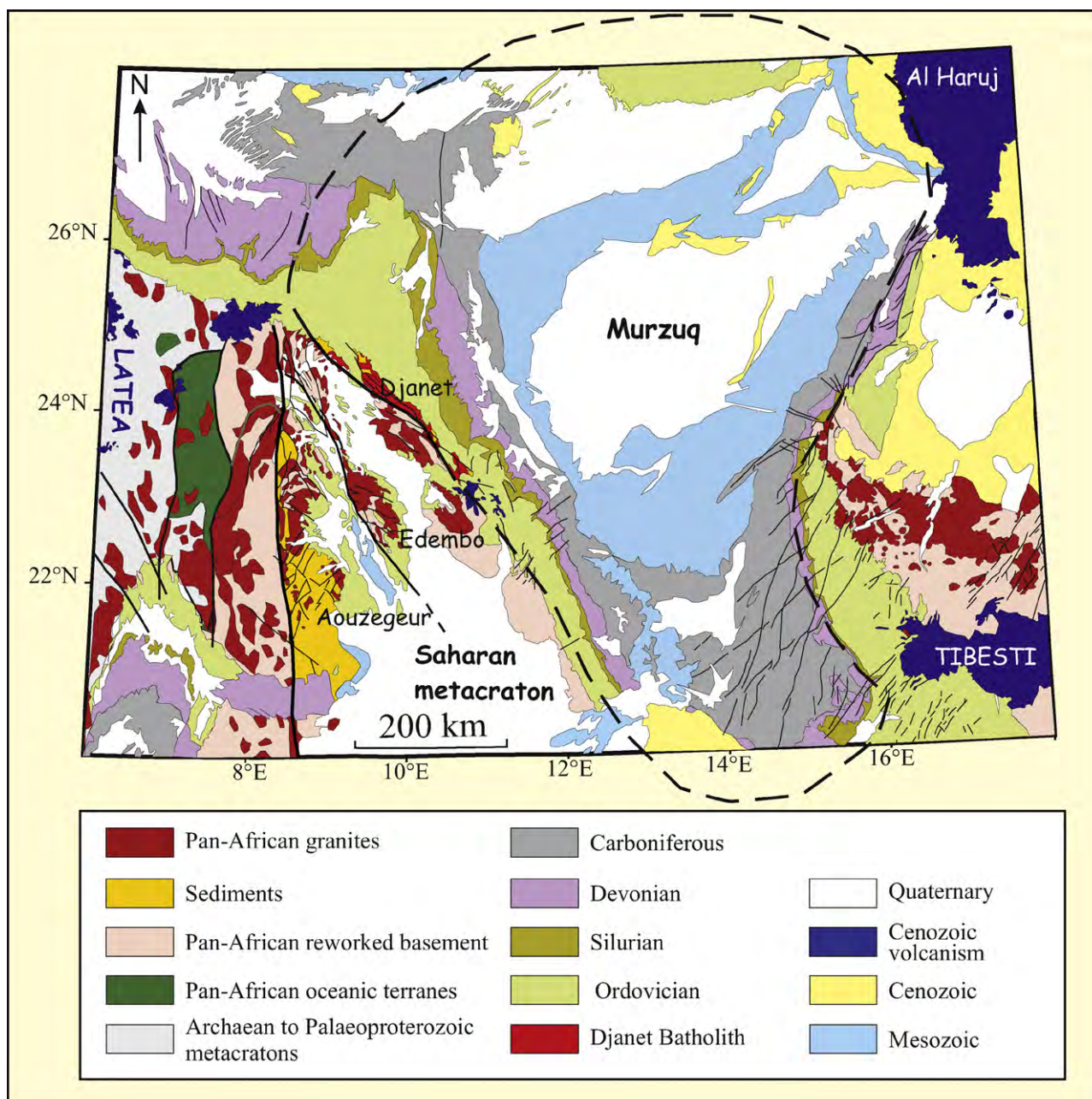


Fig. 13. Geological map showing a part of the Tuareg Shield, including the Djanet Terrane, a part of the Tibesti shield and the Murzuq craton. Modified from Lelubre (1952), Bertrand and Caby (1977), Black et al. (1994) and Le Caignec et al. (1957).

itself (Fig. 15). The basement of the Djanet Terrane would indeed be the crust of the Murzuq craton, less easy to melt if considering the thick lithosphere underneath.

Such a situation is reminiscent to the current Mongolian Altai Mountains or Russian Tien Shan situations. These mountain ranges are corresponding to an intracontinental transpressional orogen along small cratons (the Tarim, Jungar and Hangei cratons) in response to the major compression induced further south by the Indian craton (Cunningham, 2005; Zhiwei et al., 2009). As in Altai, fold-and-thrust orogenic wedge and bounding foredeep are missing in Djanet–Edembo. The crustal thickening by lower crustal inflation and northward outflow of lower crustal material invoked for Altai (Cunningham, 2005) can easily be applied to the Edembo Terrane. In Tien Shan, tomographic images of the crust and upper mantle show a thinner lithosphere below the central

part of the belt, which is compatible with an elongated lithospheric delamination (Zhiwei et al., 2009). The Edembo terrane would correspond to the central part of the Belt where delamination occurred while the Djanet Terrane would not, preventing it to partial melting and migmatitization (Fig. 15). In that model, the cause of the 570–550 Ma transpressive event that affected the Djanet and Edembo terranes must be searched beyond the Murzuq craton, maybe below the Sirte basin (Fig. 16) whose base is Cambrian (Tawadros et al., 2001) and its basement probably Neoproterozoic knowing the existence of Pan-African S-type granites to the West (Oun and Busrewil, 1987). Let us note that if the Cenozoic volcanism is abundant in the region, it is only present at the periphery of the Murzuq basin, never inside, as it is also the case for the West African craton (Fig. 16) in agreement with a cratonic structure. This Cenozoic volcanism would have been favoured by the reactivation

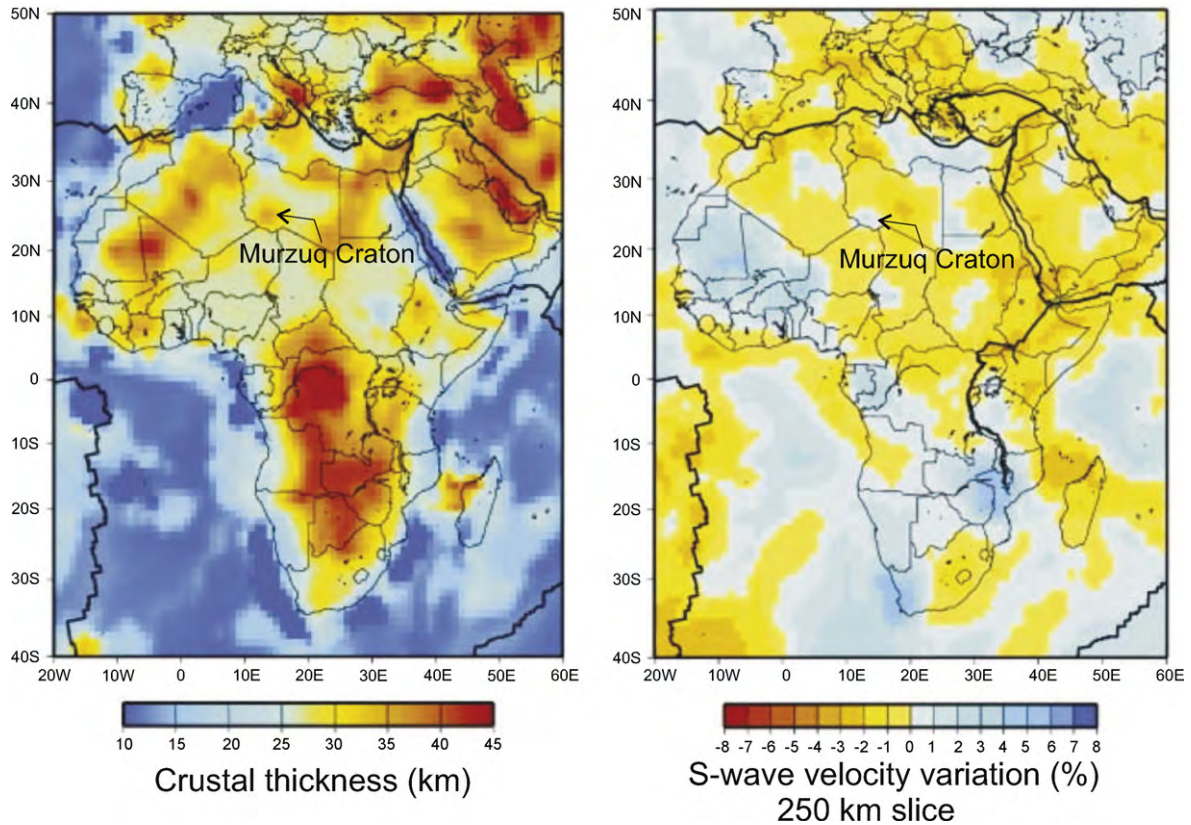


Fig. 14. Geophysical data for Africa (Pasyanos and Nyblade, 2007) showing the thick crust and the thick lithospheric mantle below the Murzuq craton.

of the metacratonic boundaries of the Murzuq craton during the Europe–Africa convergence since 38 Ma as proposed for the other West African volcanic fields (Liégeois et al., 2005).

The intracontinental magmatic, metamorphic and tectonic episode that affects the Djanet and Edembo is younger (570–550 Ma) than the Pan-African orogeny further west in the

Tuareg Shield (630–580 Ma) and is only preceded by the deposition of the sediments from the Djanet Group. It is thus not a fading episode of the Pan-African orogeny and it is not related to the collision with the West African craton. We suggest in consequence naming this orogenic event the Murzukian intracontinental episode, of late Ediacaran age.

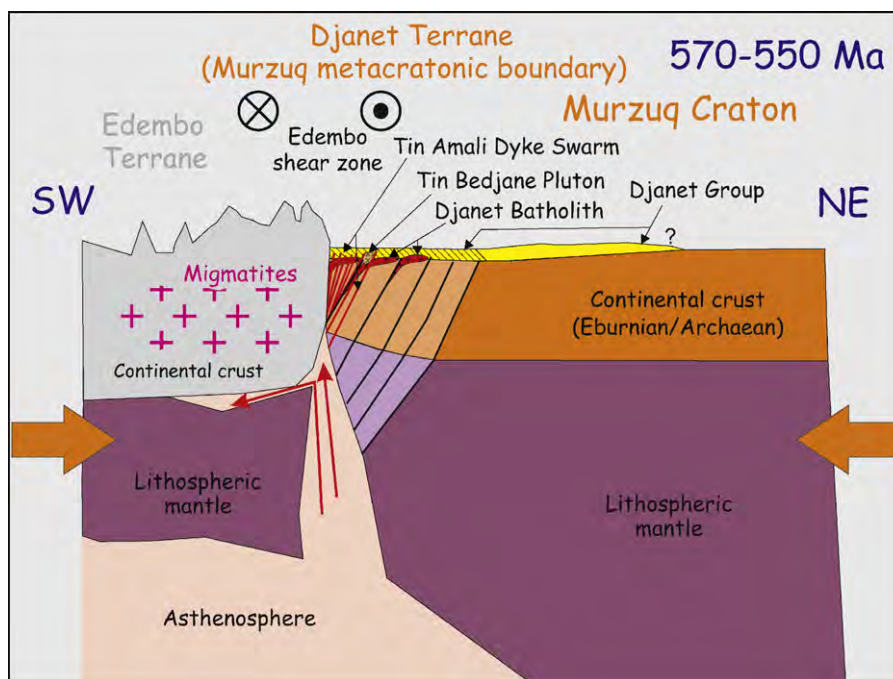


Fig. 15. Schematic model section at c. 570 Ma of the Murzuq craton, the Djanet Terrane, its metacratonic boundary and the Edembo Terrane (mobile belt).

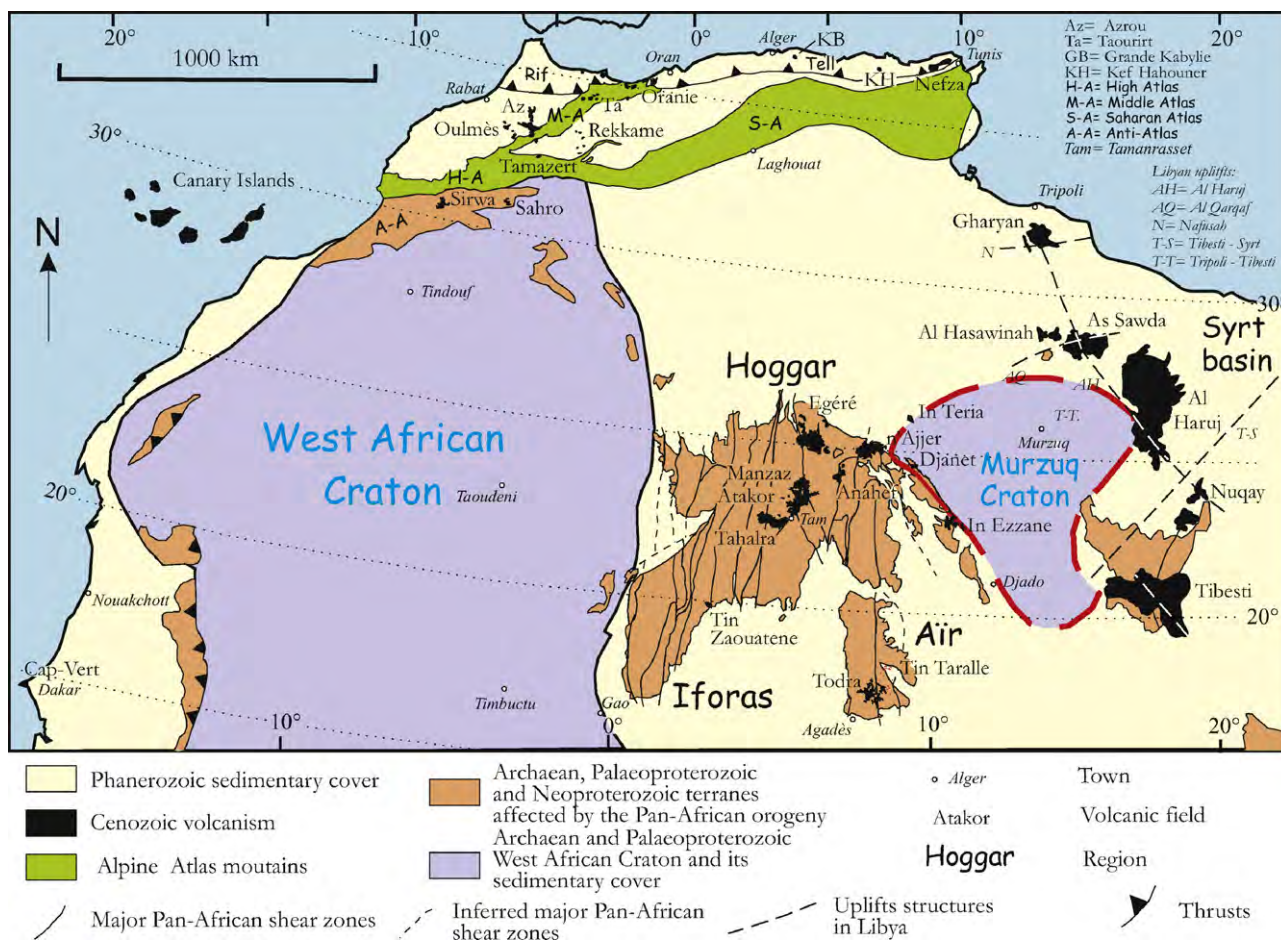


Fig. 16. The Cenozoic volcanism of West Africa (Liégeois et al., 2005) with the location of the Murzuq craton based on the Palaeozoic sediments. See text.

7. Conclusions

The geochronological results obtained in this study demonstrate that the Eastern Hoggar had not stabilized by c. 730 Ma as proposed by Cabyl and Andreopoulos-Renaud (1987) but was subjected to a late Ediacaran tectono-magmatic episode at c. 575–555 Ma. This episode is younger, distinct and unlinked to the Pan-African orogeny that occurred further west in the Tuareg Shield. We propose to name it the Murzukian intracontinental episode.

The Murzukian episode generated a transpressive deformation under greenschist conditions in the Djanet Terrane and under amphibolite-facies in the adjacent Edembo Terrane with granitoid intrusions in both terranes. The oldest recorded event in both terranes is the deposition of the Djanet Group at 580 ± 10 Ma; no oceanic rocks at all are known. Detrital zircons indicate that the source of the sediments of the Djanet Group was the Tuareg Shield. Age peaks (laser ICP-MS zircon ages) have been detected at 602 (28%), 638, 673 (26%), 735 (9%), 947 (2%), 1750 (4%), 1908 (13%), 2402 and 2438 (7%), 2650 (2%), 2800 and 2844 (2%) and 3232 (2%) Ma, with the characteristic absence of Mesoproterozoic ages.

The magmatic suites of the Djanet Terrane although volumetrically significant, occurred over a short period of time of 15 m.y. (U–Pb SHRIMP zircon ages). This includes the Djanet Batholith (571 ± 16 Ma), the high-level circular Tin Bedjane Pluton (568 ± 5 Ma) and the Tin Amali Dyke Swarm (558 ± 6 Ma). This magmatism is all high-K calc-alkaline in composition. Nd T_{DM} two-stage model ages vary from 1.30 to 2.05 Ga with a mean of 1637 ± 82 Ma for the Djanet Batholith, of 1780 ± 55 Ma for the Tin Bedjane Pluton

and of 1730 ± 17 Ma for the Tin Amali Dyke Swarm suggesting that all the magmatism of the Djanet Terrane originated from the same source, being old continental crust with some addition of juvenile mantle magma at the origin of crustal melting. The migmatitic amphibolite-facies in the Edembo Terrane occurred at the same time (568 ± 4 Ma).

We propose here the existence of a Murzuk craton just to the East, below the Murzuk basin, based on geophysical and sedimentary evidences. The Murzukian intracontinental transpressive episode would be due to the indentation of the Murzuk craton, maybe in response to what occurred beyond this craton to the NE in a similar way as is the intracontinental orogeny currently occurring in the Altai in related to the Indian collision more to the South (Cunningham, 2005).

In that model, the Djanet Terrane would be the metacratonic boundary of the lithosphere-thick Murzuq craton, only fractured and invaded by granitoids with a good preservation of the Djanet Group, a similar situation as in the metacratonic Anti-Atlas belt (Ennih and Liégeois, 2008). By opposition the Edembo Terrane has been much more remobilized and uplifted by the transpression. The high-temperature migmatitization and consequent high heat flow could be the result of a linear lithospheric delamination that occurred along the shear zone delimiting the two terranes such as proposed for Tien Shan (Zhiwei et al., 2009) and LATEA metacraton (Liégeois et al., 2003). This allowed asthenospheric uprise, supplying the heat source for melting of the crust. This melting event could be not only the source of the Edembo magmatism but also that of the magmatism of the Djanet Terrane, invading the fractured metacratonic boundary (Fig. 15). The Western Tibesti, on the SW

boundary of the Murzuq craton could be the Libyan counterpart of the Algerian Djanet Terrane.

Compared to the Tuareg Shield west of the Raghane shear zone, characterized by the Pan-African 630–580 Ma time span and N-S shear zones, the Murzukian episode is not only younger (575–555 Ma) but has a distinct NW–SE orientation marked by the shear zones of Eastern Hoggar (Fig. 1). This is explained by the role of the West African craton in the first case and by the Murzuk craton in the second case. This latter convergence could have produced far field stress constraints responsible for brittle deformation further to the west such as in Air (quartz dykes; Liégeois et al., 1994) and late magmatism such as the Taourirt granitic plutons (Azzouni-Sekkal et al., 2003).

Acknowledgements

SHRIMP work was carried on the Perth Consortium facilities at the John de Laeter Centre for Mass Spectrometry, Curtin University of Technology funded by the Australian Research Council. SEM imaging was conducted at the Centre for Microscopy and Microanalysis at the University of Western Australia. We thank Bob Thomas, Bob Stern and an anonymous reviewer for their valuable and precise comments, allowing us to strongly enhance this paper. Randall Parrish is thanked for his stimulating editorial handling.

Appendix A. Supplementary data

Supplementary data associated with this article can be found, in the online version, at doi:10.1016/j.precamres.2010.05.011.

References

- Abdallah, N., Liégeois, J.P., De Waele, B., Fezaa, N., Ouabadi, A., 2007. The Temagoussine Fe-cordierite orbicular granite (Central Hoggar, Algeria): U–Pb SHRIMP age, petrology, origin and geodynamical consequences for the late Pan-African magmatism of the Tuareg Shield. *Journal of African Earth Sciences* 49, 153–178.
- Abdelsalam, M., Liégeois, J.P., Stern, R.J., 2002. The Saharan metacraton. *Journal of African Earth Sciences* 34, 119–136.
- Acef, K., Liégeois, J.P., Ouabadi, A., Latouche, L., 2003. The Anfeg post-collisional Pan-African high-K calc-alkaline batholith (Central Hoggar, Algeria), result of the Latea microcontinent metacratonisation. *Journal of African Earth Sciences* 37, 295–311.
- Avigad, D., Sandler, A., Kolodner, K., Stern, R.J., McWilliams, M., Miller, N., Beyth, M., 2005. Mass-production of Cambro–Ordovician quartz-rich sandstone as a consequence of chemical weathering of Pan-African terranes: environmental implications. *Earth and Planetary Science Letters* 240, 818–826.
- Avigad, D., Stern, R.J., Beyth, M., Miller, N., McWilliams, M.O., 2007. Detrital zircon U–Pb geochronology of Cryogenian diamictites and Lower Paleozoic sandstone in Ethiopia (Tigrai). Age constraints on Neoproterozoic glaciation and crustal evolution of the southern Arabian–Nubian Shield. *Precambrian Research* 154, 88–106.
- Azzouni-Sekkal, A., Liégeois, J.P., Bechiri-Benmerzoug, F., Belaidi-Zinet, S., Bonin, B., 2003. The “Taourirt” magmatic province, a marker of the very end of the Pan-African orogeny in the Tuareg Shield: review of the available data and Sr–Nd isotope evidence. *Journal of African Earth Sciences* 37, 331–350.
- Bathia, M.R., 1983. Plate tectonics and geochemical composition of sandstones. *Journal of Geology* 91, 611–627.
- Bau, M., 1996. Controls on the fractionation of isovalent trace elements in magmatic and aqueous systems. Evidence from Y/Ho, Zr/Hf and lanthanide tetrad effect. *Contribution to Mineralogy and Petrology* 123, 323–333.
- Bendaoud, A., Ouzegane, K., Godard, G., Liégeois, J.P., Kienast, J.R., Bruguier, O., Drareni, A., 2008. Geochronology and metamorphic P–T–X evolution of the Eburnean granulite-facies metapelites of Tidjenouine (Central Hoggar, Algeria): witness of the LATEA metacratonic evolution. In: Ennih, N., Liégeois, J.-P. (Eds.), *The Boundaries of the West African Craton*, vol. 297. Geological Society of London. Special Publication, pp. 111–146.
- Bertrand, J.M.L., Caby, R., 1977. Carte géologique du Hoggar, Algérie. Direction des Mines de la Géologie, SONAREM, scale 1:1,000,000, 2 sheets.
- Bertrand, J.M.L., Caby, R., 1978. Geodynamic evolution of the Pan-African orogenic belt: a new interpretation of the Hoggar shield (Algerian Sahara). *Geologische Rundschau* 67, 357–388.
- Bertrand, J.M.L., Caby, R., Ducrot, J., Lancelot, J.R., Moussine-Pouchkine, A., Saadallah, A., 1978. The late Pan-African intracontinental linear fold belt of the eastern Hoggar (Central Sahara, Algeria): geology, structural development, U/Pb geochronology, tectonic implications for the Hoggar shield. *Precambrian Research* 7, 349–376.
- Bertrand, J.M., Michard, A., Boullier, A.M., Dautel, D., 1986. Structure and U/Pb geochronology of Central Hoggar (Algeria): a reappraisal of its Pan-African evolution. *Tectonics* 5, 955–972.
- Beuf, S., Biju-Duval, B., De Charpal, O., Rognon, P., Gariel, O., Bennacef, A., 1971. Les grès du Paléozoïque inférieur au Sahara. Publication IFP, Collection “Science et techniques du pétrole”, Paris, 464 pp.
- Black, R., Liégeois, J.P., 1993. Cratons, mobile belts, alkaline rocks and continental lithospheric mantle: the Pan-African testimony. *Journal Geological Society London* 150, 89–98.
- Black, R., Caby, R., Moussine-Pouchkine, A., Bayer, R., Bertrand, J.M.L., Boullier, A.M., Fabre, J., Lesquer, A., 1979. Evidence for late Precambrian plate tectonics in West Africa. *Nature* 278, 223–227.
- Black, R., Latouche, L., Liégeois, J.P., Caby, R., Bertrand, J.M., 1994. Pan-African displaced terranes in the Tuareg Shield (Central Sahara). *Geology* 22, 641–644.
- Boullier, A.M., Rocci, G., Cosson, Y., 1991. La chaîne pan-africaine d’Aouzegeur en Aïr (Niger): un trait majeur du bouclier touareg. *Comptes rendus Académie des Sciences de Paris* 313, 63–68.
- Caby, R., 1996. A review of the In Ouzzal granulitic terrane (Tuareg shield, Algeria): its significance within the Pan-African Trans-Saharan belt. *Journal of Metamorphic Geology* 14, 659–666.
- Caby, R., 2003. Terrane assembly and geodynamic evolution of central-western Hoggar: a synthesis. *Journal of African Earth Science* 37, 133–159.
- Caby, R., Andreopoulos-Renaud, U., 1983. Age à 1800 Ma du magmatisme sub-alkalin associés aux métasédiments monocycliques de la chaîne pan-africaine du Sahara central. *Journal of African Earth Sciences* 1, 193–197.
- Caby, R., Andreopoulos-Renaud, U., 1987. Le Hoggar oriental, bloc cratonisé à 730 Ma dans la chaîne pan-africaine du Nord du continent africain. *Precambrian Research* 36, 335–344.
- Caby, R., Andreopoulos-Renaud, U., Gravelle, M., 1982. Cadre géologique et géochronologie U/Pb sur zircon des batholites précoces dans le segment pan-africain du Hoggar central (Algérie). *Bulletin de la Société Géologique de France* 7, 876–882.
- Cunningham, D., 2005. Active intracontinental transpressional mountain building in the Mongolian Altai: defining a new class of orogen. *Earth and Planetary Science Letters* 240, 436–444.
- De Waele, B., Liégeois, J.P., Nemchin, A.A., Tembo, F., 2006. Isotopic and geochemical evidence of Proterozoic episodic crustal reworking within the Irumide belt of South-Central Africa, the southern metacratonic boundary of an Archaean Bangweulu craton. *Precambrian Research* 148, 225–256.
- Djellit, H., Bellon, H., Ouabadi, A., Derder, M.E.M., Henry, B., Bayou, B., Khaldi, A., Baziz, K., Merahi, M.K., 2006. Âge $^{40}\text{K}/^{40}\text{Ar}$ Carbonifère inférieur, du magmatisme basique filonien du synclinal paléozoïque de Tin Serririne, Sud-Est du Hoggar (Algérie). *Comptes Rendus Geoscience* 338, 624–631.
- El Makhrouf, A.A., 1998. Tectonic interpretation of Jabal Eghel area and its regional application to Tibesti orogenic belt south central Libya (S.P.L.A.J.). *Journal of African Earth Sciences* 7, 945–967.
- Ennih, N., Liégeois, J.P., 2008. The boundaries of the West African craton, with a special reference to the basement of the Moroccan metacratonic Anti-Atlas belt. In: Ennih, N., Liégeois, J.-P. (Eds.), *The Boundaries of the West African Craton*, vol. 297. Geological Society of London. Special Publication, pp. 1–17.
- Frost, B.R., Barnes, C.G., Collins, W.J., Arculus, R.J., Ellis, D.J., Frost, C.D., 2001. A geochemical classification for granitic rocks. *Journal of Petrology* 42, 2033–2048.
- Gromet, L.P., Haskin, L.A., Korotev, R.L., Dymek, R.F., 1984. The “North American shale composite”: its compilation, major and trace element characteristics. *Geochimica et Cosmochimica Acta* 48, 2469–2482.
- Henry, B., Liégeois, J.P., Nouar, O., Derder, M.E.M., Bayou, B., Bruguier, O., Ouabadi, A., Belhai, D., Amenna, M., Hemmi, A., Ayache, M., 2009. Repeated granitoid intrusions during the Neoproterozoic along the western boundary of the Saharan metacraton, Eastern Hoggar, Tuareg shield, Algeria: an AMS and U–Pb zircon age study. *Tectonophysics* 474, 417–434.
- Hsieh, P.S., Chen, C.H., Yang, H.J., Lee, C.Y., 2008. Petrogenesis of the Nanling Mountains granites from South China: constraints from systematic apatite geochemistry and whole-rock geochemical and Sr–Nd isotope compositions. *Journal of Asian Earth Sciences* 33, 428–451.
- Jahn, B.M., Caby, R., Monié, P., 2001. The oldest UHP eclogites of the World: age of UHP metamorphism, nature of protoliths and tectonic implications. *Chemical Geology* 178, 143–158.
- Küster, D., Liégeois, J.P., Matukov, D., Sergeev, S., Lucassen, F., 2008. Zircon geochronology and Sr, Nd, Pb isotope geochemistry of granitoids from Bayuda Desert and Sabaloka (Sudan): evidence for a Bayudian event (920–900 Ma) preceding the Pan-African orogenic cycle (860–590 Ma) at the eastern boundary of the Saharan Metacraton. *Precambrian Research* 164, 16–39.
- Le Caignec, J., Harel, M., Didier, J., Illy, P., 1957. Reports of the BRMA (Bureau de Recherches Minières de l’Algérie) for Djanet area, Mission Illy (Hoggar 1956–1957), Feuilles au 1/200 000: Fort Charlet et Tin Alkoum.
- Lelubre, M., 1952. Recherche sur la géologie de l’Ahaggar central et occidental (Sahara centrale). *Bulletin Service géologique de l’Algérie* 22, tome 1, 354 p.; tome 2, 387 pp.
- Le Maitre, R.W., Streckeisen, A., Zanettin, B., Le Bas, M.J., Bonin, B., Bateman, P., Bellieni, G., Dudek, A., Efremova, S., Keller, J., Lameyre, J., Sabine, P.A., Scmid, R., Sorensen, H., Woolley, A.R., 2002. *Igneous Rocks: A Classification and Glossary of Terms: Recommendations of the International Union of Geological Sciences. Subcommission on the Systematics of Igneous Rocks*. Cambridge University Press, 236 pp.

- Liégeois, J.P., 2005. The Pan-African evolution of the Tuareg shield, with reference to the Neoproterozoic granitoids and the Cenozoic volcanism. In: Séminaire de géologie et de métallogénie des massifs du Hoggar et des Eglab, Tamanrasset, Algérie.
- Liégeois, J.P., Black, R., 1987. Alkaline magmatism subsequent to collision in the Pan-African belt of the Adrar des Iforas. In: Fitton, J.G., Upton, B.G.J. (Eds.), *Alkaline igneous Rocks*, vol. 30. The Geological Society, Blackwell Scientific Publication, pp. 381–401.
- Liégeois, J.P., Stern, R.J., 2010. Sr–Nd isotopes and geochemistry of granite-gneiss complexes from the Meatiq and Hafafit domes, Eastern Desert, Egypt: no evidence for pre-Neoproterozoic crust. *Journal of African Earth Sciences* 57, 31–40.
- Liégeois, J.P., Bertrand, J.M., Black, R., 1987. The subduction- and collision-related Pan-African composite batholith of the Adrar des Iforas (Mali): a review. In: Kinnaird, J., Bowden, P. (Eds.), *African Geology Review*. J. Wiley, London, pp. 185–211. *Geological Journal* 22, 185–211.
- Liégeois, J.P., Black, R., Navez, J., Latouche, L., 1994. Early and late Pan-African orogenies in the Air assembly of terranes (Tuareg Shield, Niger). *Precambrian Research* 67, 59–88.
- Liégeois, J.P., Navez, J., Hertogen, J., Black, R., 1998. Contrasting origin of post-collisional high-K calc-alkaline and shoshonitic versus alkaline and peralkaline granitoids. *Lithos* 45, 1–28.
- Liégeois, J.P., Latouche, L., Boughrara, M., Navez, J., Guiraud, M., 2003. The LATEA metacraton (Central Hoggar, Tuareg Shield, Algeria): behaviour of an old passive margin during the Pan-African orogeny. *Journal of African Earth Sciences* 37, 161–190.
- Liégeois, J.P., Benhallou, A., Azzouni-Sekkal, A., Yahiaoui, R., Bonin, B., 2005. The Hoggar swell and volcanism: reactivation of the Precambrian Tuareg Shield during Alpine convergence and West African Cenozoic volcanism. In: Foulger, G.R., Natland, J.H., Presnall, D.C., Anderson, D.L. (Eds.), *Plates, Plumes and Paradigms*, vol. 388. Geological Society of America Special Paper, pp. 379–400.
- Moreau, C., Demaiiffe, D., Bellion, Y., Boullier, A.M., 1994. A tectonic model for the location of the Paleozoic ring-complexes in Air (Niger, West Africa). *Tectonophysics* 234, 129–146.
- Moussa, E.M.M., Stern, R.J., Manton, W.I., Ali, K.A., 2008. SHRIMP zircon dating and Sm/Nd isotopic investigations of Neoproterozoic granitoids, Eastern Desert, Egypt. *Precambrian Research* 160, 341–356.
- Oun, K.M., Busrewil, M.T., 1987. S-type granite from Jabal Al Hasawnah, west central Libya. *Journal of African Earth Sciences* 6, 851–856.
- Ouzegane, K., Kienast, J.R., Bendaoud, A., Drareni, A., 2003. A review of Archaean and Paleoproterozoic evolution of the In Ouzzal granulitic terrane (Western Hoggar, Algeria). *Journal of African Earth Science* 37, 207–227.
- Pasyanos, M.E., Nyblade, A.A., 2007. A top to bottom lithospheric study of Africa and Arabia. *Tectonophysics* 444, 27–44.
- Pearce, J.A., 1982. Role of the Sub-continental Lithosphere in Magma Genesis at Active Continental Margins. *Continental Basalts and Mantle Xenoliths*. Shiva Publication, Cheshire, U.K, pp. 230–249.
- Peucat, J.J., Capdevila, R., Drareni, A., Choukroune, P., Fanning, C.M., Bernard-Griffiths, J., Fourcade, S., 1996. Major and trace element geochemistry and isotope (Sr, Nd, Pb, O) systematic of an Archaean basement involved in 2.0 Ga very high-temperature (1000 °C) metamorphic event: In Ouzzal Massif, Hoggar, Algeria. *Journal of metamorphic Geology* 14, 667–692.
- Peucat, J.J., Drareni, A., Latouche, L., Deloule, E., Vidal, P., 2003. U–Pb zircon (TIMS and SIMS) and Sm–Nd whole rock geochronology of the Gour Oumalelen granulitic basement, Hoggar massif, Tuareg Shield, Algeria. *Journal of African Earth Science* 37, 229–239.
- Rickwood, P.C., 1989. Boundary lines within petrologic diagrams which use oxides of major and minor elements. *Lithos* 22, 247–264.
- Roser, B.P., Korsch, R.J., 1986. Determination of tectonic setting of sandstone-mudstone suite using SiO₂ content and K₂O/Na₂O ratios. *Geological Journal* 94, 635–650.
- Streckeisen, A., Le Maitre, R.W.L., 1979. A chemical approximation to the modal QAPP Classification of the igneous rocks. *Neues Jahrbuch für Mineralogie Abteilung* 136, 169–206.
- Suayah, I.B., Miller, J.S., Miller, B.V., Bayer, T.M., Rogers, J.J.W., 2006. Tectonic significance of Late Neoproterozoic granites from the Tibesti massif in southern Libya inferred from Sr and Nd isotopes and U–Pb zircon data. *Journal African Earth Sciences* 44, 561–570.
- Sun, S.S., 1980. Lead isotopic study of young volcanic rocks from mid-ocean ridges, ocean islands and island arcs. *Philosophical Transactions Royal Society London* A297, 409–445.
- Taylor, S.R., Mc Lennan, S.M., 1985. *The continental Crust: Its Composition and Evolution*. Blackwell, Oxford, 312 pp.
- Tawadros, E., Rasul, S.M., Elzaroug, R., 2001. Petrography and playnology of quartzites in the Sirte Basin, Central Libya. *Journal African Earth Sciences* 32, 373–390.
- Veksler, I.V., Dorfman, A.M., Kamenetsky, M., Dulski, P., Dingwell, D.B., 2005. Partitioning of lanthanides and Y between immiscible silicate and fluoride melts, fluorite and cryolite and the origin of the lanthanide tetrad effect in igneous rocks. *Geochimica et Cosmochimica Acta* 69, 2847–2860.
- Zhiwei, L., Roecker, S., Zhihai, L., Bin, W., Haitao, W., Schelochkov, G., Bragin, V., 2009. Tomographic image of the crust and upper mantle beneath the western Tien Shan from the MANAS broadband deployment: possible evidence for lithospheric delamination. *Tectonophysics* 477, 49–57.